Hybrid Mathematical Modelling of Three-Phase Flow in Porous Media: Application to Water-Alternating-Gas Injection

Afzali Shokufe, Zendehboudi Sohrab, Mohammadzadeh Omid, Rezaei Nima

DOI: 10.1016/j.jngse.2021.103966

Hybrid Mathematical Modelling of Three-Phase Flow in Porous Media: Application to Water-Alternating-Gas Injection

Shokufe Afzali[1], Sohrab Zendehboudi[1], Omid Mohammadzadeh[1], Nima Rezaei[2]

[1]Faculty of Engineering and Applied Science, Memorial University, St. John's, NL, Canada

[2]Department of Separation Science, Lappeenranta-Lahti University of Technology, Finland

Abstract

Machine learning algorithms are extensively used to reduce the complexity of applied problems in various fields, including energy. Accurate prediction of the performance of water alternating gas (WAG) as an enhanced oil recovery (EOR) process is of great importance in the optimal management of the hydrocarbon resources. In the current work, a hybrid mathematical model is proposed for the near-immiscible WAG process. We use data-driven sub-models, including least square support vector machine (LSSVM) and adaptive neuro-fuzzy inference system (ANFIS) in series with an empirical model (EM) and a first principle model (FPM) to study three-phase flow in porous media. The LSSVM and ANFIS sub-models predict the two-phase water-oil, gas-oil, and gas-water relative permeabilities. The outputs from these models are supplied to the empirical models (EMs) to estimate the three-phase relative permeabilities for oil, gas, and water phases. The model developed using LSSVM shows a better prediction performance in estimating the relative permeabilities, compared to that using ANFIS. The relative importance parameter analysis shows that for the LSSVM sub-model, water saturation is the most influencing input parameter for the gas-water and oil-water systems while for the gas-oil system, gas saturation is the most important input parameter. Using the models proposed in this work, some hybrid models are developed to forecast the ultimate recovery factor (RF) in the testing phase. The predicted ultimate RF values are 92.0%, 91.6%, and 82.9% for the correlation-based EM-FPM, LSSVM-EM-FPM, and ANFIS-EM-FPM hybrid models, respectively, in comparison to the measured ultimate RF value of 93.6% after three cycles of water- and gas-injection. Among the proposed hybrid models, the LSSVM-EM-FPM model significantly removes the non-linearity of the two-phase relative permeabilities. In general, the LSSVM-EM-FPM hybrid model possess the same level of accuracy as that of the EM-FPM hybrid model, but with significantly less model complexity and non-linearity. Thus, the LSSVM-EM-FPM hybrid model can be used in demanding applications such as optimization and control of this oil recovery process, leading to a better resource management.

Keywords: WAG injection; Three-phase relative permeability; LSSVM; ANFIS; Machine learning; Recovery factor

1 Introduction

The WAG injection has been successfully field tested as a promising EOR technique. Through controlling the frontal mobility, the WAG injection process features a lower residual oil saturation compared to traditional waterflooding or gas injection especially in miscible condition [1]. Generally, four mechanisms are responsible for enhanced productivity of the WAG injection process, including: 1) changing the oil density as well as reducing its viscosity as a result of the interactions between the oil phase and the light components of the injecting gas phase, depending on the temperature, pressure, and composition of the oil and gas phases, 2) changing the three-phase relative permeability of the phases that result more stable fluid fronts, 3) trapping of the non-wetting phase(i.e. gas), and 4) reducing the interfacial tension (IFT) between the phases upon compositional changes, leading to lower residual oil saturations [1].

During a WAG injection process, some complex displacement patterns occur due to highly non-monotonic saturation variations of all three phases [2]. Since the WAG process involves subsequent injections of different fluids, simulation of the process performance is more complicated than that of a typical three-phase flow system [3]. It is thus important to further explore the vital characteristics of the WAG process such as relationships between relative permeabilities of the phases while studying the flow behavior in such complex systems.

In a WAG flooding process, directional hysteresis occurs in the magnitudes of the relative permeability during the changes in saturation history between the subsequent imbibition and drainage displacements in the system [4-6]. Three-phase relative permeability data are necessary to model the distribution and transport of oil, water, and, gas in porous media; and to evaluate the pressure and velocity distribution of the available phases [7]. Relative permeability functions integrate the effects fluid and rock properties, and fluid saturations in porous media [8]. Skauge and Larsen [9] used dynamic WAG injection experiments and measured unsteady three-phase relative permeability values using consecutive cycles of water-and-gas injections for different porous media wetting conditions. In each cycle, the relative permeability of all the phases showed irreversible hysteresis effects. The gas phase saturation profiles

(as the most non-wetting phase) caused more hysteresis effects in all porous media compared to the wetting phase.

Obtaining two-phase relative permeability data is more straightforward than those of the three-phase, as the lower number of phases decreases the available saturation paths [10]. However, a three-phase flow system has infinite number of saturation paths that makes it difficult to estimate the three-phase relative permeability values [11,12]. In the literature, two main approaches are followed to estimate the three-phase relative permeability data: 1) direct measurements using coreflooding experiments, and 2) predictions made from two-phase relative permeability data. In the first approach, the three-phase relative permeability values are obtained using steady-state or unsteady-state experiments. In addition, there are various empirical correlations to estimate the three-phase relative permeability values using the two-phase data [13]. One of the primitive correlations that estimate the three-phase relative permeability was introduced by Stone, that is widely known as "Stone I" model [14]. In this model, the three-phase relative permeability data are predicted based on measured two-phase data points. The Stone I model assumes that water and gas are separated in the system, and the oil bank displacements by water and gas are two independent processes [14]. However, the error associated with the Stone I model (and similar models) is high, making these relative permeability correlations unreliable for modelling the three-phase flow in porous media. Therefore, several investigations are performed to enhance the accuracy of the existing three-phase relative permeability models against experimental data [15, 16]. These studies also revealed that there is no single model that can fit to the experimental data from different sources which is not surprising, considering variation in the rock and fluid properties involved in different experimental studies. Two-phase relative permeabilities are non-linear functions of the phase saturations, which are influenced by various parameters such as phase saturation history [17], pore size distribution, pore structure [18], wettability, permeability and porosity [19], overburden pressure, the IFT between fluids, fluid properties (e.g., viscosity and density) [20], initial wetting phase saturation, and the flow rate [21]. The two-phase relative permeabilities do not only control the fluid flow and saturation distribution in two-phase systems, but their values and behavior also significantly affect the fluid flow in three-phase systems. However, the relative influence of the two-phase relative permeabilities and the impact of rock and fluid properties in three-phase systems have not been clearly understood and quantified in the literature [22].

Smart tools such as artificial neural network (ANN) models enable us with robust toolboxes to conduct non-linear and multidimensional interpolations. These models are being extensively applied in various

sectors from biology to engineering. However, the application of ANN (and connectionist) models in the petroleum industry and specifically in EOR processes is still in its infancy. A WAG injection process involves complicated three-phase flow including the hysteresis effects. During this cyclic injection process, infinite saturation paths are created. This adds further difficulties to predict all possible variations of three-phase relative permeability curves at each imbibition/drainage displacement. In this work, we utilize two of the powerful smart tools, namely LSSVM and ANFIS, for estimation of the three-phase relative permeabilities based on the two-phase data. The proposed models appear to be promising in determination of the two-phase relative permeability values to avoid repetitive high-cost blind laboratory tests, especially during a complex three-phase flow such as WAG injection process.

Vapnik [23] proposed the idea of support vector machine (SVM) to address typical problems and limitations that are encountered in the ANN modeling, such as overfitting, convergence to local minima, and inconsistence or unrepeatable results [24]. Additionally, although the structure of the SVM is simpler than ANN (less model parameters and no hidden nodes), it converges to a global minima. The SVM network topology and is only obtained through the training stage and does not demand a priori knowledge about its structure [25, 26]. In general, the SVM model develops a robust machine learning approach that uses statistical learning theory, leading to reliable generalization of the performance [27-29]. -Due to the extensive uncertainty, complexity, and non-linear behaviors associated with various data and properties reported in the petroleum industry, the SVM model is considered as a reliable tool in dealing with these challenges [30]. There are modified versions of the SVM model that are applied for data analysis in the oil and gas industry. For instance, Fayazi et al. predicted natural gas viscosity using least square support vector machine (LSSVM) model [31]. In another work, Esmaeili et al. used supervised (learning) LSSVM model to predict the effect of temperature on two-phase oil-water relative permeability data [22]. The LSSVM model has also been used for other oil and gas related applications such as predicting the phase equilibrium conditions of clathrate hydrate[32], modelling freezing point depression of electrolyte solutions[33], calculating minimum miscibility pressure for CO_2-oil systems[34], and estimating dew point pressure for a gas condensate system[34].

The fuzzy neural network models benefit from the learning capability in the ANNs and knowledge demonstration capability of the fuzzy logic [35]. Adaptive neuro-fuzzy inference system (ANFIS) eliminates the drawbacks of the neural networks, such as the lack of transparency in explaining the main decision, and the weaknesses involved in the learning stage of fuzzy logic. ANFIS is able to predict systems with acceptable accuracy in various subjects/disciplines such as engineering, medicine,

transportation, business, and economics [36]. However, ANFIS also faces major limitations such as high dimensionality and training complexity, which impose restrictions on problems with large datasets [37,38]. ANFIS algorithm has been extensively used in engineering research studies to predict, for instance, permeability and porosity [39, 40], injection profile and well placement [41, 42], oil viscosity [43], minimum miscibility pressure (MMP) [44, 45], asphaltene precipitation [46], reservoir oil solution gas-oil ratio, and oil recovery factor [47, 48], gas volume fraction in two-phase flow [49], gas velocity in two phase flow [50], nanofluid convective flow and temperature [51-53], velocity of heated nanofluids in a porous pipe [54], physical multiphase flow properties [55], and unloading gradient pressure in continuous gas-lift processes [56]. In a study, Roghanian et al. used ANFIS and identified the complex relation between rock and fluid properties and water-oil relative permeability key points including: maximum water and oil relative permeability values, cross point saturation, and cross point relative permeability [57].

In this work, the LSSVM, ANFIS, and a correlation-based empirical model (EM) are used to determine the two-phase relative permeability values in three systems of oil-water, oil-gas, and gas-water. The predicted values are then embedded in a first principle model (FPM) of WAG flooding process to estimate the ultimate recovery factor for comparison with some experimental data. We structured the paper as follows: after the introduction, we provide the mathematical framework, including the mathematical model and numerical solution. The theoretical framework of data acquisition and analysis, and the training procedure of the ANFIS and LSSVM models are then given. We also discuss the limitations associated with the applied models. After evaluating the two-phase relative permeability predictions by the ANFIS and LSSVM models, we discuss the oil recovery factor, three-phase relative permeability of all the phases, and the relative importance of all the input parameters. The models are then applied to a case study and the predictions are compared with the experimental results. Finally, the main conclusions drawn from the results are listed.

2 Theoretical Frameworks of LSSVM and ANFIS Models

2.1 LSSVM model

For a specific set of the experimental data $\{(x_1, y_1), (x_2, y_2), \dots, (x_N, y_N)\}$ in which $x_i \in R^n$ and $y_i \in R$ are the input and output variables, respectively, the following relationship is applied by the SVM algorithm to evaluate the separation plane [59-61]:

$$y = w^T.\varphi(x) + b \tag{1}$$

where w is weight factor; $\varphi(x)$ is a non-linear function; T is matrix transpose operation; and b is bias term. Through this non-linear function, the data (x_i) are mapped into the n-dimensional feature space [62]. When the given dataset is divided into two linearly separable classes (1 and 2), the constraints in Eq. (2) applies[34, 61]. For $y_i = +1$, the input data x_i belong to class 1 and for $y_i = -1$ the input data belong to class 2.

$$\begin{cases} w^T.\varphi(x) + b \geq +1 & y_i = +1 \\ w^T.\varphi(x) + b \leq -1 & y_i = -1 \end{cases} \tag{2}$$

The margin is set as a distance between the plane passing through the data points of class 1 or 2 with values of $y_i = +1$ and $y_i = -1$, respectively. The constraints presented in Eq. (2) can be generalized as seen in Eq. (3) for a separable case. Using a slack variable ($\zeta_i \geq 0$), Cortes and Vapnik extended the inequality constraints for a non-separable case (see Eqs. (4)– (5)) [62].

$$y_i[w^T.\varphi(x_i) + b] \geq +1, \quad i = 1,2,3,\dots,N \tag{3}$$

$$y_i[w^T.\varphi(x_i) + b] \geq 1 - \zeta_i, \quad i = 1,2,3,\dots,N \tag{4}$$

$$\zeta_i \geq 0, \quad i = 1,2,3,\dots,N \tag{5}$$

Similar to other conventional optimization algorithms, the LSSVM algorithm uses constraints to introduce objective or cost function(s). An objective function (also called, cost function) can be developed (see Eq. (6)), using the constraints and a constant value C (which is a positive and real number); the cost function provides a trade-off between the classification error and margin [31]:

$$Cost(w,\zeta) = \frac{1}{2}w^T.w + \frac{C}{2}\sum_{i-1}^{N}\zeta_i^p \tag{6}$$

Using the Lagrangian multipliers α and β, and by imposing its derivate equal to zero, the constraints minimization (in Eqs. (4) and (6)) changes to an unconstraint minimization as seen in Eq (7) [31]:

$$U(w,b,\alpha,\beta,\zeta) = \frac{1}{2}w^T.w + \frac{C}{2}\sum_{i-1}^{N}\zeta_i^p - \sum_{i=1}^{N}\alpha_i(y_i[w^T.\varphi(x_i) + b] - 1 + \zeta_i) - \sum_{i=1}^{N}\beta_i\zeta_i \tag{7}$$

The LSSVM algorithm is a modified version of the SVM model in which a linear set of equations are solved instead of the quadratic equations of the SVM. Hence, a new cost function (Eq. (8)) is obtained in which the parameter ζ is the regression error and γ is the model tuning parameter [22]:

$$R(w,\zeta) = \frac{1}{2}w^T.w + \frac{\gamma}{2}\sum_{i-1}^{N}\zeta_i^2 \quad (8)$$

In the LSSVM algorithm, similar constraints to those of the SVM algorithm (Eq. (4)) are applied which include the equality constraints instead of the inequality constraint (Eq. (3)), as given below [22]:

$$y_i[w^T.\varphi(x) + b] = 1 - \zeta_i, \quad i = 1,2,3,\dots,N \quad (9)$$

The following Lagrangian function is developed that uses the Lagrangian multiplier α [29, 63]:

$$U(w,b,\alpha,\beta,\zeta) = \frac{1}{2}w^T.w + \frac{\gamma}{2}\sum_{i-1}^{N}\zeta_i^2 - \sum_{i=1}^{N}\alpha_i(y_i[w^T.\varphi(x) + b] - 1 + \zeta_i) \quad (10)$$

where α can be either a positive or a negative value depending on the formulation of the LSSVM algorithm. The optimum point is met where the derivatives of Eq. (10) with respect to $b, \alpha,$ and ζ become zero. The following equations are resulted from the derivation of Eq. (10) [29, 63]:

$$\begin{cases} \frac{\partial U}{\partial w} = 0 \quad => w = \sum_{i=1}^{N}\alpha_i y_i\varphi(x_i) \\ \frac{\partial U}{\partial b} = 0 \quad => \sum_{i=1}^{N}\alpha_i y_i = 0 \\ \frac{\partial U}{\partial \zeta_i} = 0 \quad => \alpha_i = \gamma\zeta_i, i = 1,2,\dots,N \\ \frac{\partial U}{\partial \alpha_i} = 0 \quad => y_i[w^T.\varphi(x_i) + b] = 1 - \zeta_i,, i = 1,2,\dots,N \end{cases} \quad (11)$$

$$\begin{bmatrix} o & 1_N^T \\ 1_N & \Omega + \gamma^{-1}I_N \end{bmatrix}\begin{bmatrix} b \\ \alpha \end{bmatrix} = \begin{bmatrix} 0 \\ Y \end{bmatrix} \quad (12)$$

Eq. (12) is Karush-Kuhn-Trucker equation in which $\alpha = [\alpha_1, \alpha_2, \dots, \alpha_N]^T$, $y = [y_1, y_2, \dots, y_N]^T$, and $1 = [1,1,\dots,1]^T$; furthermore, $\Omega \in R^{N\times N}$ represents the kernel matrix with a size of $N \times N$, and I_N refers to the identity matrix. In Eq. (12), w and ζ parameters are removed. The transformation (ψ) of the input variables to feature space is simplified by using kernel function $K(x_i, x_j)$:

$$\Omega_{ij} = \psi^T(x_i)\psi(x_j) = K(x_i, x_j) \quad (13)$$

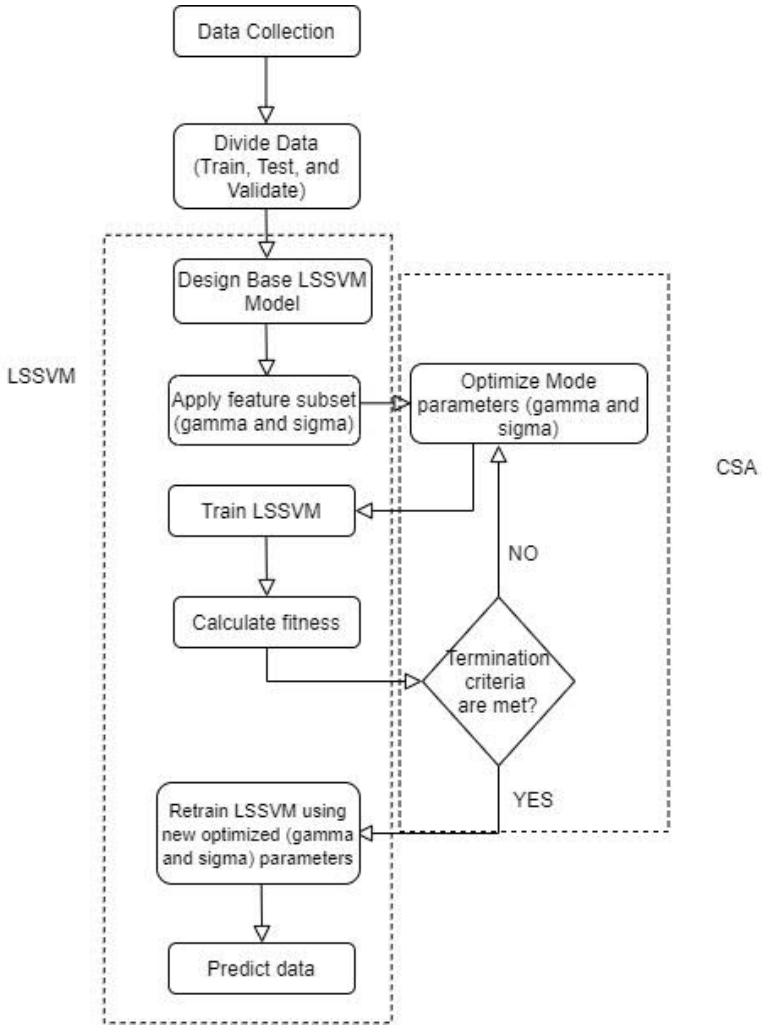

Figure 1:A schematic of LSSVM-CSA model used in current work [64].

Numerous kernel function are proposed in the literature, such as polynomial, linear, spline, and radial basis function (RBF) [65-68]. In the current study, we use the RBF kernel function (Eq. (14)) in which $\sigma^2$is the squared variance of the Gaussian distribution function that is be minimized in the SVM algorithm [22].

$$K(x, x_i) = \exp\left(\frac{-\|x_i - x\|^2}{\sigma^2}\right) \tag{14}$$

Figure 1 shows a schematic of the general algorithm of a LSSVM-CSA applied in this study.

2.2 ANFIS model

The ANFIS model hybridizes the fuzzy inference system (FIS) and ANN to minimize the drawbacks associated with each of these stand-alone models [38]. ANFIS is an adaptive multi-layer feed forward network which is originally applied for forecasting target parameters in nonlinear systems [69, 70]. The ANFIS model structure, consisting of nodes in five different layers [71], is based on fuzzy values being determined during the training stage [72]. The flowchart for the ANFIS model, including its hybrid optimization algorithm, is illustrated in Figure 2.

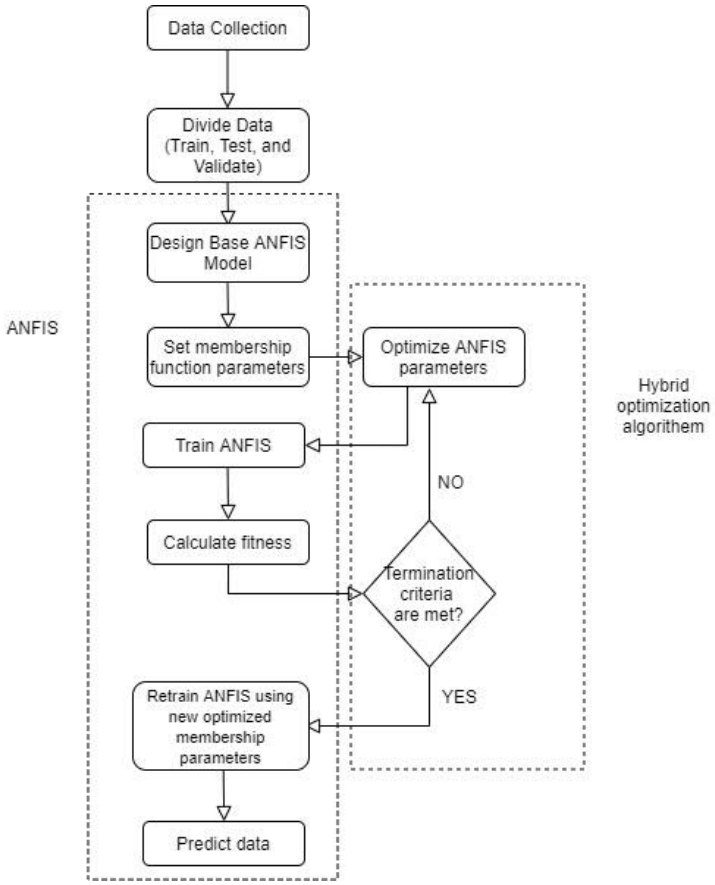

Figure 2: Simplified flowchart of the ANFIS model optimized by a hybrid algorithm [64].

In this approach, each node is designed using its membership function. The O_i^j represents the output of the i^{th} node in the layer j. For example, in the first layer where j=1, the i^{th} node refers to an adaptive node

with the input of x (or y). The linguistic label attributed for this node is referred as A_i (or B_{i-2}). The membership function for a given node is formed as follows [73]:

$$O_i^1 = \mu_{Ai}(x); \quad i = 1,2$$
or,
$$O_i^1 = \mu_{Bi-2}(y); \quad i = 3,4 \tag{15}$$

The O_i^1 symbolizes the membership function of a given fuzzy set A (A_1, A_2, B_1 or B_2) that calculates the step where the input (x or y) correlates to the quantifier A. The membership functions (MFs) can also be obtained (for A and B) by a generalized bell function as follows [73]:

$$\mu_{Ai}(x) = \frac{1}{1+\left\|\frac{x-r_i}{p_i}\right\|^{2q_i}} \tag{16}$$

where p_i, q_i, and r_i represent the set parameters. The shape of functions depends on these set parameters. For the next layer (j=2), the inputs are multiplied using the nodes, and their product is represented as [73]:

$$O_i^2 = w_i \mu_{Ai}(x)\mu_{Bi}(y); \quad i = 1,2 \tag{17}$$

Each product node resembles the rules of firing strength. In the third layer, also known as the normalization layer, the ratio of firing strength of node i^{th} to the summation of all rules firing strengths is determined as follows [73]:

$$O_i^3 = \overline{w}_i = \frac{w_i}{w_1+w_2}, \quad i = 1,2 \tag{18}$$

In the fourth layer, the i^{th} node computes the portion of the i^{th} rule to the total output, defined by the following equation [73]:

$$O_i^4 = \overline{w}_i z_i = \overline{w}_i(a_i x + b_i y + c_i), \quad i = 1,2 \tag{19}$$

where $\overline{w}_i$ refers to the normalized firing strength (the output from the 3rd layer); a_i, b_i, and c_i denote the set parameters which are known as the consequent parameters.

In the fifth layer, the final output is calculated by the summation of all entering signals to a node as given below [73]:

$$O_i^5 = \sum_i \overline{w}_i z_i = \frac{\sum_i w_i z_i}{\sum_i wi} \tag{20}$$

3 WAG Injection Model Characteristics

The WAG injection process is a three-phase flow application in porous medium, in which both the wetting (water) and non-wetting (gas) phases are injected sequentially [74, 75]. The numerical modelling of WAG injection process is challenged by the complexities related to the three-phase flow and its cyclic injection nature.

3.1 Mathematical model development

In this research, we use a 1D core and apply implicit-pressure explicit-saturation (IMPES) method as the first principal model (FPM) for the WAG injection process. Details of the mathematical foundation for the three phase flow in porous medium are described in our previous work [76].

The three-phase relative permeability values are related to the saturation history as well as the saturation distribution. The saturation history of each phase causes relative permeability hysteresis; there are reported laboratory hysteresis results for from saturation history in two-phase and (to a less extent) in the three-phase tests [6, 77, 78]. The majority of the reported three-phase relative permeability models that are available in the literature infer the three-phase results from the two-phase relative permeability data. Stone and Baker models are among the most commonly used relative permeability correlations that do not perform well in calculating the three phase relative permeability data [16]. The three-phase flow parameters (e.g., relative permeability and capillary pressure) should be obtained as a function of saturations of the various phases in the system [79-82]. In the current mathematical modeling study, three-phase relative permeability model by Shahverdi and Sohrabi is used [83]. This model accounts for the three-phase hysteresis effects in which the three-phase relative permeability values of phase *i* (k_{ri}^{3ph}) is defined as [83]:

$$k_{ro}^{3ph}(s_w, s_g) = \frac{\overline{s_o}}{(1-\overline{s_g})(1-\overline{s_w})}[k_{row}k_{rwg} + k_{rog}k_{rgw}] \quad (21)$$

$$k_{rw}^{3ph}(s_o, s_g) = \frac{\overline{s_w}}{(1-\overline{s_g})(1-\overline{s_o})}[k_{rwo}k_{rog} + k_{rwg}k_{rgo}] \quad (22)$$

$$k_{rg}^{3ph}(s_w, s_o) = \frac{\overline{s_g}}{(1-\overline{s_o})(1-\overline{s_w})}[k_{rgo}k_{row} + k_{rgw}k_{rwo}] \quad (23)$$

where *i* and *j* subscriptions are the three available phases (e.g., oil, water, or gas), and k_{rij} refers to the two-phase relative permeability of phase *i* in the presence of phase *j*. The s_i stands for the saturation of

phase *i*. In the current study, the two-phase relative permeability values are calculated using correlation-based, LSSVM, and ANFIS models as described in the next sections.

The $\overline{s_i}$ is the normalized saturation for the phase *i*, that is affected by the initial saturation values and the injection cycle (i.e., gas injection, or water injection), as given below [83]:

$$\overline{s_g} = \frac{s_g - s_g^*}{1 - s_w^* - s_o^* - s_g^*} \tag{24}$$

$$\overline{s_o} = \frac{s_o - s_o^*}{1 - s_w^* - s_o^* - s_g^*} \tag{25}$$

$$\overline{s_w} = \frac{s_w - s_w^*}{1 - s_w^* - s_o^* - s_g^*} \tag{26}$$

In Eqs. (24) to (26), the s_i^* values are defined for different phases.

Table 1 summarises the three-phase relative permeability model parameters (see Eqs. (21) to (26)) that are used in our simulation. In Table 1, s_α^{start} is the starting point saturation of phase α when injection cycle is started; and s_{gt} and s_{ot} denote the trapped/residual saturations of gas and oil, respectively.

Table 1: The parameters used in the three-phase relative permeability model in the porous medium [83].

Three-phase relative permeability	Model parameters	WAG injection cycle		
		Gas	Oil	Water
k_{rg}^{3ph}	s_g^*	s_g^{start}	s_{gt}	s_{gt}
	s_w^*	s_{wc}	s_{wc}	s_w^{start}
	s_o^*	0	s_o^{start}	s_{ot}
k_{ro}^{3ph}	s_g^*	0	s_{gt}	s_{gt}
	s_w^*	s_{wc}	s_{wc}	s_w^{start}
	s_o^*	s_{org}	s_o^{start}	s_{ot}
k_{rw}^{3ph}	s_g^*	0	0	0
	s_w^*	s_{wc}	s_{wc}	s_{wc}
	s_o^*	0	0	0

In this work, the three-phase flow in a 5 cm diameter core plug in the context of the WAG injection process is simulated. In the modeling phase, the assumption of 1D flow is rationale because the effect of gravity is not expected to be significant due to the small diameter of the core sample. The two-phase permeability values are obtained through smart tools (ANFIS and LSSVM) or EMs. During each injection cycle, the parameters of the two-phase relative permeability model should be tuned, when using

EMs. The two-phase relative permeability data calculated using the optimized EMs will then be embedded in the three-phase relative permeability model to calculate the three-phase relative permeability of each phase.

Figure 3 depicts a schematic of the flowchart applied in this study.

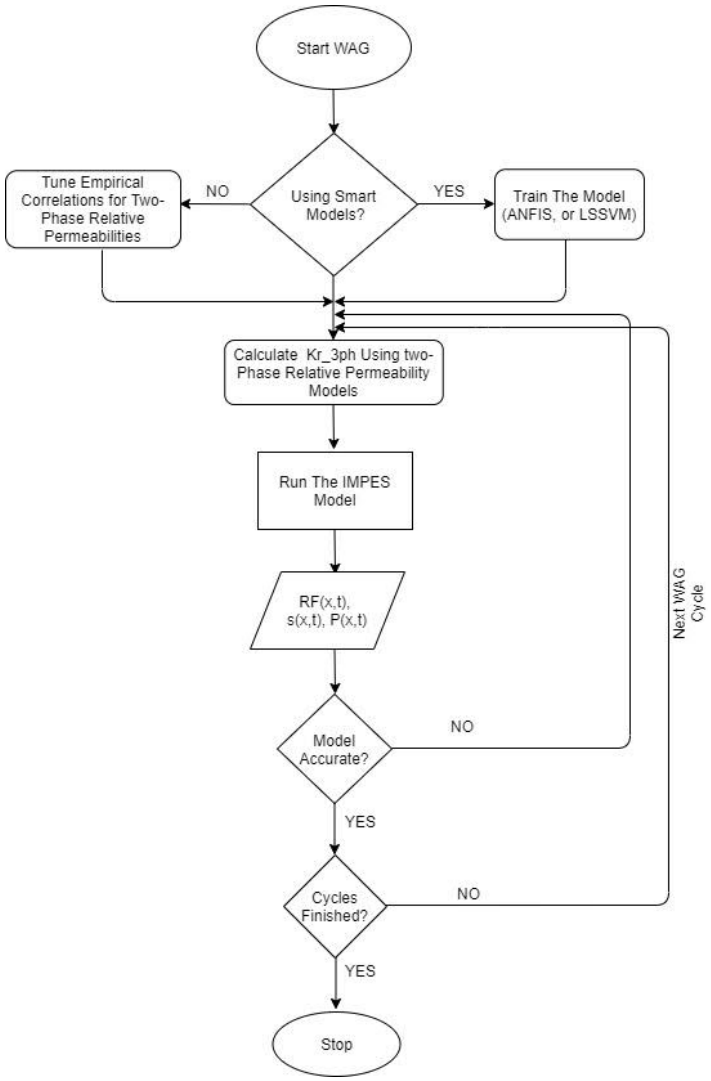

Figure 3: WAG injection modeling flowchart applied in current study.

3.2 Empirical models (EMs)

EMs are important tools to calculate relative permeability values for a given wetting condition. The EMs are only applicable within the range of experimental conditions based on which they have been developed; therefore, generalization beyond the experimental conditions is risky. This lack of

generalization capability can be a major source of error in predicting the relative permeability data for the desire processes. However, availability of these correlations, in addition to their capability of being easily tuned for various processes and conditions, have made them practical tools to predict relative permeability values. In this research, two EMs are employed to calculate the two-phase relative permeabilities in order to be embedded later in the three-phase relative permeability model proposed by Shahverdi et al. [16]. The three-phase relative permeability data calculated from Shahverdi et al. [16] model are then used in a FPM for a three-cycle WAG injection process. Among the numerous suggested EMs in the literature, two of the most known models are Mualem's model (Eqs. (27)-(29)), which is a modified version of Van Genuchten model, and Hirasaki's model (Eqs. (30)-(32)) [84, 85].

$$k_{rw}(s_w) = \overline{s_w}^{0.5}\left(1-\left(1-\overline{s_w}^{\frac{1}{m}}\right)^{m}\right)^{2} \tag{27}$$

$$k_{rn}(s_n) = \overline{s_n}^{\frac{1}{3}}\left(1-\left(1-\overline{s_n}^{\frac{1}{m}}\right)\right)^{2m} \tag{28}$$

$$\overline{s_\alpha} = \frac{s_\alpha - s_{\alpha r}}{1-\sum_\alpha s_{\alpha r}} \tag{29}$$

where the subscription *w* denotes the wetting phase; *n* refers to the non-wetting phase; $s_{\alpha r}$ symbolizes the residual saturation of the phase α; k_{rn} and k_{rw} denotes the two-phase relative permeability of the non-wet and wetting phase, respectively; and m is the model parameter which is obtained through optimization.

$$k_{rw} = k_{rw}^0 S_D^{\,n_w} \tag{30}$$

$$k_{rn} = k_{rnw}^0 (1-S_D)^{n_n} \tag{31}$$

$$S_D = \frac{S_w - S_{wi}}{1-S_{wi}-S_{nr}} \tag{32}$$

Where k_{rw} and k_{rn} denote the two-phase relative permeability values for the wetting phase and non-wetting phase, respectively; k_{rw}^0 and k_{rn}^0 are the end-point relative permeability values for the wetting phase and non-wetting phase, respectively; s_w is the saturation of the wetting phase; s_{wi} and s_{nr} refer to the initial wetting saturation and residual saturation of the non-wetting phases, respectively; and n_w and n_n refer to the model parameters for the wetting and non-wetting phases, respectively, which are obtained by fitting the model to the experimental data.

4 Modelling of WAG Injection Process Using LSSVM and ANFIS Algorithms

4.1 Data acquisition, quality check, and analysis

In machine learning applications, the capability of the model in terms of robustness, accuracy, and universality highly depends on the quality of the input data [86-88]. A review of the previous studies shows that relative permeabilities are related to rock properties (permeability and porosity) [17-18], fluid properties (saturation, or viscosity) [20], and operating conditions (pressure and temperature) [21, 22]. In the current study, we use different datasets for three systems of oil-water, oil-gas, and gas-water in order to predict the two-phase relative permeability values for each phase. A total number of 2,116 raw datapoints are borrowed from the literature. After performing an initial raw data quality check and analysis, several datasets are discarded due to inconsistencies (10 datasets from the oil-gas system, 3 datasets from the oil-water system, and 8 datasets from the gas-water system). Indeed, the modeling is conducted with a total number of 1,457 data points. The details of the database utilized in each system are described in Table 2. All the collected data belong to strongly water-wet sandstone rocks to match the wettability conditions of the proposed case study.

Table 2: The details of database utilized in each system.

Input	Gas-Oil (510 data points)		Oil-Water (626 data points)		Gas-Water (321 data points)	
	Variable	Range	Variable	Range	Variable	Range
1	S_{wc}	0.03–0.50	S_w	0.052–1	P(kPa)	0.3–24233
2	S_{org}	0.05–0.48	T(˚C)	21.1–200	K (mD)	0.004–3515
3	S_{gc}	0.006–0.25	μ_o (cP)	0.419–1190	ϕ	0.0416–0.37
4	k (mD)	1.48–3650	μ_w (cP)	0.136–1.1	T (˚C)	25–120
5	ϕ	0.063–0.39	K (mD)	152–95000	S_w	0.1–1
6	S_g	0–0.95				

ANFIS Training phase. In the ANFIS algorithm, the input and output data are first normalized in the range of -1 to +1 to make the predictions computationally efficient and enhance their accuracy. In this study, we use Takagi-Sugeno fuzzy model for the ANFIS algorithm. The optimization parameters for the relative permeability prediction by ANFIS model are listed in Table 3 for all three systems.

Table 3: Optimization parameters used in the ANFIS model for oil-water, oil-gas, and water-gas systems.

ANFIS parameter	System		
	Oil-Water	Oil-Gas	Gas-Water
Fuzzy structure	Takagi-Sugeno	Takagi-Sugeno	Takagi-Sugeno
Initial FIS for training	genfis2	genfis2	genfis2
Membership function type	Gaussian	Gaussian	Gaussian
Output membership function	Linear	Linear	Linear
Cluster center's influence range	0.7	0.5	0.4
Number of inputs	5	6	5
Number of outputs	1	1	1
Training maximum epoch number	200	200	200
Initial step size	0.1	0.1	0.1
Step size decrease rate	0.9	0.9	0.9
Step size increase rate	1.1	1.1	1.1

LSSVM Training phase. The LSSVM model contains two adjustable parameters (σ^2, and γ) which are optimized during the prediction process. In the current study, we use coupled simulated annealing (CSA) optimization method. The optimization search algorithm is repeated to converge to the global-optima. By having the optimum values of σ and γ, the unknown vector (α) and the bias term (b) are computed for relative permeabilities in all three-systems (two-phase relative permeability).

4.2 Advantages and limitations of the models

Overall, the AI modelling tools are classified into three main categories: the black-box (data-driven) models which include all the connectionist tools; the white-box (first principal) models; and the grey-box (hybrid) models combined with either white-box or black-box models [89]. The black-box models provide a higher computational speed and efficiency compared to other models while requiring minimum knowledge of the targeted phenomena. The black-box models, however, are heavily dependent on the data. One of the main limitations of the black-box models is their low capability in extrapolating data [90]. On the other hand, the white-box models are highly dependent on the physics and the type of the phenomena being modeled; they are able to provide a deep understanding of the processes/phenomena since they can be developed before starting the modelling procedure.

The accuracy of a model is limited by its assumptions. The major advantages and limitations of the applied models, in the current study, are listed in Table 4.

Table 4: Limitations and advantages of the smart tools used in this study.

Model	Advantages	Disadvantages
LSSVM	• High accuracy and generalization capabilities • No over-fitting or under-fitting problem [99] • Applicability in systems with limited data points [100] • No local minima; leads to a global optimum. • Less complexity in the model structure compared to ANN [101] • No need for prior knowledge of the network topology. • Contains only two adjustable parameters (σ^2 and γ). • High computational speed and high efficiency [102]	• Lack of the sparsity limits the method for large scale processes [103]. • Employing the sum square error without regularization results in less accuracy in data prediction.
ANFIS	• Capturing the non-linear structure of a process • High adaption capability • Rapid learning capacity • Handling both numerical and linguistic knowledge. • Employing the ANN ability to classify data and identifying parameters. • Applicable in data involving crisp input and crisp output [43]	• High computational cost due to the complex structure and gradient learning which is more significant while dealing with large inputs. • Implies a trade-off between interpretability and accuracy. • Limited number and type of membership function [35].

5 Results and Discussions

In three-phase flow systems of oil-water, oil-gas, and gas-water, we first predict the two-phase relative permeability values and use them in the three-phase relative permeability model. In this section, we first present the criteria applied to evaluate the prediction performance of different proposed methods. Second, the models are optimized, and the trained models are hybridized with the FPM to estimate the ultimate recovery factor as an important measure of the WAG recovery performance. The reliability and precision of the predictions are then assessed through comparison with the experimental data, for both the ultimate recovery factor and the three-phase relative permeability values.

The reliability and robustness of the predictions derived from the developed models are examined using various statistical quality and error analysis measures such as coefficient of determination (R^2), mean error (ME), standard deviation (std), and root mean square error (RMSE). These statistical parameters are defined for a dataset of N samples, each expressed as (x_1, x_2,… , x_k, y) where k is the number of input features; x_j is the independent input j variable; and y denotes the target value according to the following equations:

$$R^2 = 1 - \frac{\sum_{i=1}^{N}(y_i-(y_p)_i)^2}{\sum_{i=1}^{N}((y_p)_i-\bar{y}_i)^2} \quad (33)$$

$$Error = y_i - (y_p)_i \quad (34)$$

$$ME = \frac{\sum_{i=1}^{N}(Error_i)}{N} \quad (35)$$

$$std = \sqrt{\frac{\sum_{i=1}^{N}(Error - ME)^2}{N-1}} \quad (36)$$

$$RMSE = \sqrt{\frac{\sum_{i=1}^{N}(y_i - (y_p)_i)^2}{N}} \quad (37)$$

where y_i is the output variable for the i^{th} sample data, and $(y_p)_i$ represents the corresponding output value predicted by the model. The R^2 parameter measures how much of the variations in the data is explained by the correlation; a good fit is represented by an R^2 value close to 1. The *std* is a measure of the amount of variation or dispersion of the data. The *RMSE* and *ME* measure the prediction accuracy, and the error values close to zero are desired.

We also use the following objective function (OF) that relates the predicted recovery factor values to the experimental data at the end of each cycle:

$$OF = \sum_i \frac{|RF_{prd}(i) - RF_{target}(i)|}{RF_{target}(i)} \quad (38)$$

5.1 Evaluation of the two-phase relative permeability prediction models

To predict the two-phase relative permeability values for a system, the independent input variables (described in Table 2) are embedded into the developed models (hybrid LSSVM-CSA and ANFIS). We use the CSA optimization technique to optimize the LSSVM model parameters (σ and γ) as listed in Table . The RBF is also applied in the LSSVM algorithm as the kernel function with the optimized σ and γ values. The statistical quality measures for the two-phase relative permeability predictions are presented in Table .

Table 5: Values of the optimized γ and σ parameters for the two-phase relative permeability predictions made using the LSSVM-CSA algorithm.

Relative permeability	Parameter	
	σ	γ
k_{row}	1.37990	35885.0
k_{rwo}	0.48102	703.0
k_{rog}	4.81019	2.05
k_{rgo}	0.09347	1.6987
k_{rwg}	0.65554	30.7757812
k_{rgw}	2.3409	64.79675

Table 6: The statistical quality measurements for the ANFIS and LSSVM-CSA models.

System	Statistical parameter	ANFIS						LSSVM-CSA					
		$(k_r)_{non-wet}$			$(k_r)_{wet}$			$(k_r)_{non-wet}$			$(k_r)_{wet}$		
		Training	Test	Validate	Training	Test	Validate	Training	Test	Validate	Training	Test	Validate
Oil-Water	Standard error	0.0735	0.06726	0.03270	0.01867	0.24867	0.14028	0.01846	0.04732	0.03709	0.00507	0.01826	0.01679
	Mean error	1.19e-08	4.81e-04	5.96e-03	-2.31e-07	4.81e-03	1.72e-02	-1.01e-13	-6.20e-3	-1.04e-2	2.12e-16	-4.71e-4	-5.68e-3
	RMSE	0.0150	0.0415	0.0177	0.0391	0.0943	0.0873	0.0184	0.0475	0.0382	0.0051	0.0188	0.0176
	R^2	0.9838	0.9820	0.9954	0.9827	0.9684	0.9763	0.9997	0.9987	0.9987	0.9995	0.9968	0.9939
Gas-Water	Standard error	0.09883	0.07584	0.05963	0.03112	0.07612	0.27639	0.01284	0.02660	0.02710	0.01888	0.04880	0.07047
	Mean error	-1.16e-06	1.43e-03	-6.62e-02	-2.23e-08	-1.33e-03	-1.62e-03	-9.60e-09	7.36e-4	-2.48e-4	2.47e-08	1.42e-4	1.56e-3
	RMSE	0.02457	0.02580	0.01542	0.04002	0.01849	0.21482	0.01279	0.02729	0.02646	0.01880	0.04770	0.0706063
	R^2	0.9151	0.9541	0.9946	0.9874	0.9940	0.9758	0.9898	0.9727	0.9917	0.9898	0.9892	0.9936
Gas-Oil	Standard error	0.02560	0.06592	0.01131	0.01717	0.08530	0.08269	0.006267	0.01891	0.00625	0.01650	0.08250	0.07958
	Mean error	-5.75e-08	7.70e-3	3.10e-2	7.04e-08	2.00e-03	-9.21e-02	-9.42e-14	8.35e-3	-1.92e-3	9.23e-18	2.89e-3	-8.83e-3
	RMSE	0.04220	0.03176	0.02574	0.07311	0.06051	0.08999	0.06258	0.04935	0.06182	0.01650	0.08210	0.07910
	R^2	0.9650	0.9781	0.9963	0.9606	0.9841	0.9928	0.9966	0.9953	0.9939	0.9847	0.9893	0.9958

The values of R^2 for both the developed models are close to 1 for all the two-phase fluid flow systems, demonstrating an excellent fit of the predicted values to the experimental data. The higher R^2 values associated with the LSSVM-CSA model predictions for all the fluid flow systems suggest the superiority of this model over the ANFIS model. The regression plots for the two-phase flow systems are presented in Figure 4–6. According to these plots and the statistical analysis measures presented in Table , both models are well trained; the LSSVM-CSA model is more accurate in predicting the target values of the experimental data in the training phase, which results in smaller mean error values.

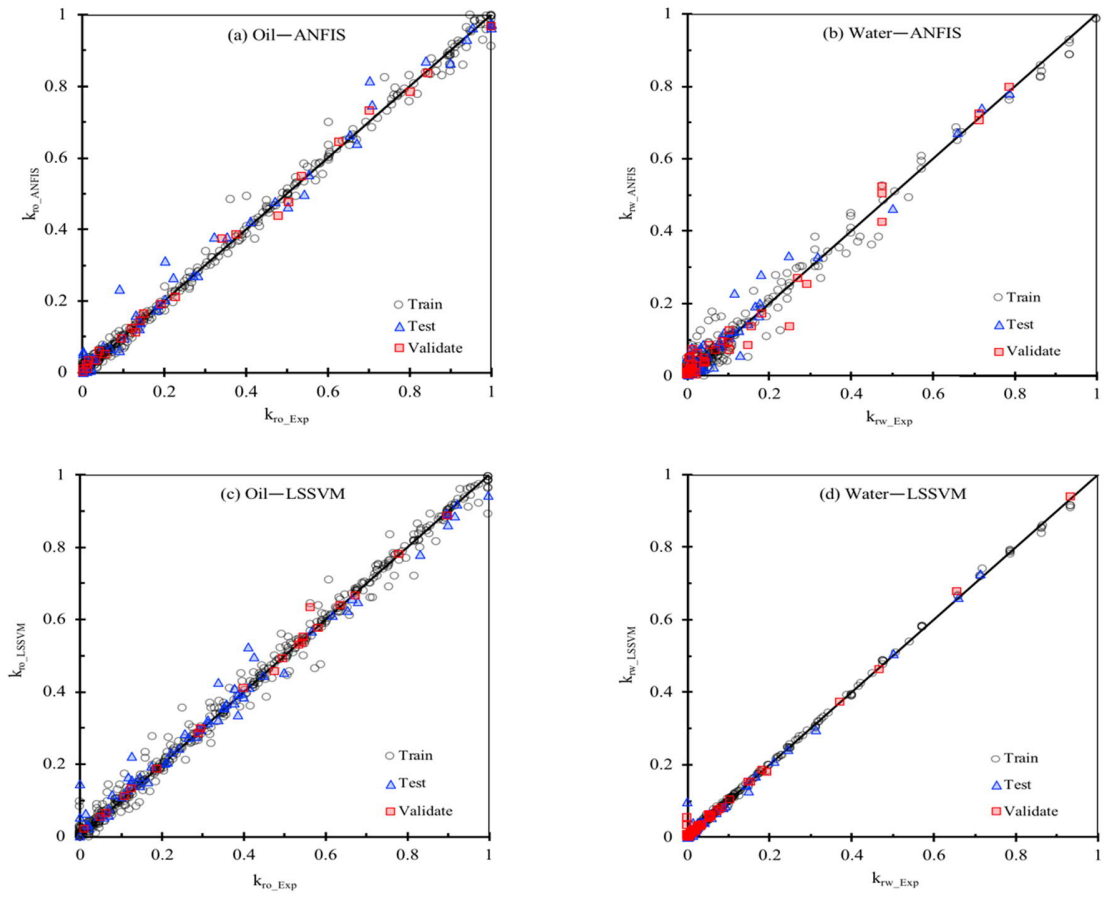

Figure 4: Regression plots for the oil-water flow system, displaying predicted versus measured (a) oil relative permeability using ANFIS model, (b) water relative permeability using ANFIS model, (c) oil relative permeability using LSSVM-CSA model, and (d) water relative permeability using LSSVM-CSA model.

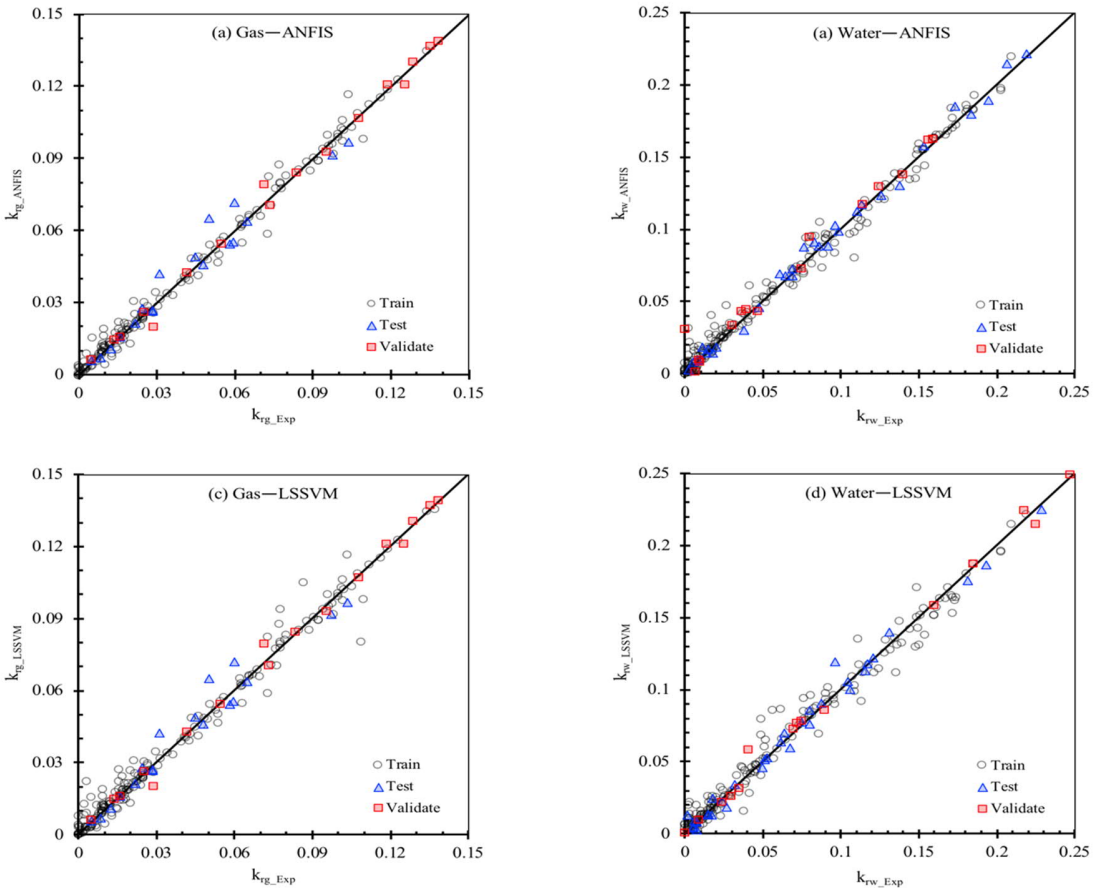

Figure 5: Regression plots for the gas-water flow system, displaying predicted versus measured (a) gas relative permeability using ANFIS model, (b) water relative permeability using ANFIS model, (c) gas relative permeability using LSSVM-CSA model, and (d) water relative permeability using LSSVM-CSA model.

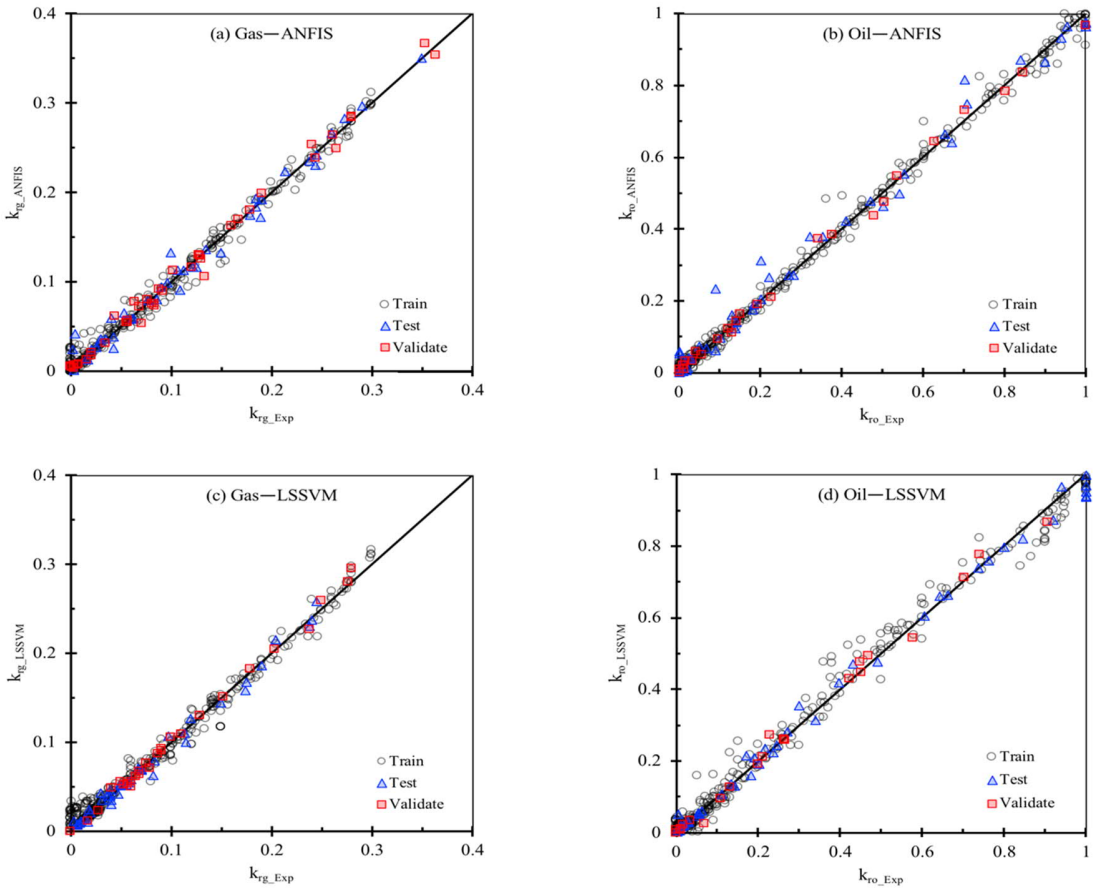

Figure 6: Regression plots for the gas-oil flow system, displaying predicted versus measured (a): gas relative permeability using ANFIS model, (b) oil relative permeability using ANFIS model, (c) gas relative permeability using LSSVM-CSA model, and (d) oil relative permeability using LSSVM-CSA model.

5.2 Evaluation of the models in predicting WAG injection ultimate recovery factor

To evaluate the performance of the developed black-box models (i.e. LSSVM-CSA and ANFIS) as well as that of the correlation-based EM (EM-FPM) model, the calculated values of the two-phase relative permeability are compared with the experimental data of a WAG injection process, containing three consecutive cycles in which water and gas are injected. In the selected experiment, the WAG injection process was conducted in a strongly water-wet porous medium, starting with a primary waterflooding stage (WI1) where no initial gas was present (i.e. s_{gi}=0). The process was then continued with the first gas injection stage (GI1). The consecutive water and gas injection

processes were continued three times. The process was terminated after the third gas injection stage (GI3) during which no significant oil production occurred. The WAG injection process was performed at a WAG ratio of 1:1, i.e. the water and gas injection flow rates were equal and set at q=25 cm^3/hr.

The plot of recovery factor versus the dimensionless time based on the predictions and experimental data is presented in Figure 7. The data associated with this plot are provided in Table 7.

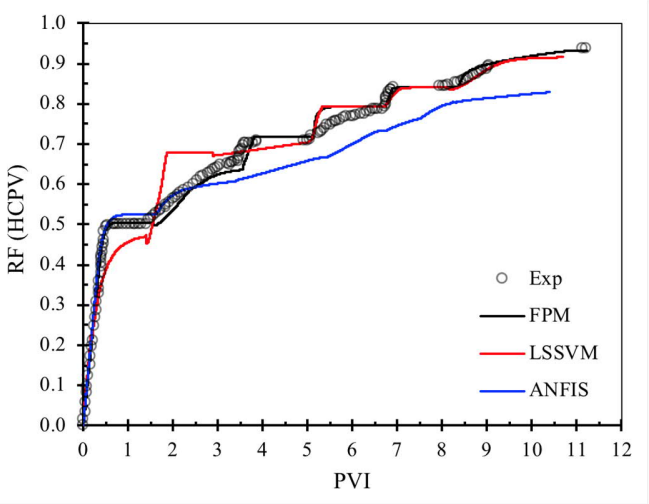

Figure 7: Comparison between the predicted versus measured *RF* values (q=25 cm^3/hr, WAG ratio=1).

Table 7: The predicted and experimentally measured RF values for the WAG injection process in a water-wet medium. Experimental data are from Fatemi et al. [91].

Cycle	Process	RF_{End} (HCPV)				Relative error in RF_{End}			Max relative error			Processing Time (s)	
		Exp	Model	LSSVM	ANFIS	Model	LSSVM	ANFIS	Model	LSSVM	ANFIS	LSSVM	ANFIS
1	WF1	0.4997	0.5008	0.4750	0.5294	-0.0022	0.04943	-0.0594	0.01575	0.12625	-0.05203	60	300
	GI1	0.6559	0.6464	0.6783	0.6098	0.01448	-0.0342	0.0703	0.0509	-0.2082	0.07121		
2	WF2	0.7201	0.7194	0.7017	0.6588	0.00097	0.02555	0.0851	-0.0172	-0.0302	0.11533	75	480
	GI2	0.7912	0.7937	0.7927	0.7318	-0.0032	-0.0019	0.0751	0.01369	-0.0635	0.10658		
3	WF3	0.8509	0.8430	0.8414	0.8047	0.00929	0.01117	0.0543	0.01019	2.46E-05	0.1151	75	480
	GI3	0.9358	0.9200	0.9157	0.8288	0.01688	0.02148	0.11434	0.01160	0.01457	0.0894		

By the end of the primary waterflooding stage (WI1), 50% of the initial oil in place is recovered based on the experimental data. The numerical simulation model, developed based on two-phase relative permeability correlation, is able to predict a RF of 50.08% at the end of the WI1 stage, implying the excellent accuracy of the numerical simulation model. The ANFIS model, however, has a less accuracy compared to the numerical simulation model, and results in a RF value of 53.94% at the end of the WI1 stage with a breakthrough time of PVI=0.566. The LSSVM-CSA model, on the other hand, underestimates the RF at the end of WI1 stage (i.e. 47.50%) as well as the breakthrough time (i.e. PVI=0.406).

When the first gas injection stage starts, the models need to account for the presence of three phases that are simultaneously flowing in the porous medium, using the three-phase capillary pressure and relative permeability models. At the end of the first cycle (i.e. end of the GI1 stage), the correlation-based numerical simulation model predicts a RF of 64.64%, which is in an excellent agreement with the experimental RF value of 65.59%. The LSSVM-CSA and ANFIS models predict the RF values at the end of the first injection cycle at 67.83% and 60.98%, respectively. Two additional injection cycles are then implemented, and the measured as well as predicted RF values at the end of each cycle, along with the statistical quality measures of relative error and maximum relative error, with respect to the experimental data, are all listed in Table 7. The maximum relative error specifies the highest relative error of all the instantaneous *RF* values during each cycle. The relative error, however, shows the relative error involved in estimating the ultimate recovery factor values (RF_{End}) using each model during each injection process (GI or WI). The WAG injection process is continued for a total dimensionless time of 11.24 *PVI*. Considering the accuracy measures and predicted values of the RF at each cycle of the WAG injection (Table and Figure 7), the ANFIS model is found to be the less successful method in predicting the correct trend and values of the experimental data; this results in significant error values. The greatest relative error in predicted ultimate RF, i.e. 11.43%, is associated with this model. Also, the greatest maximum error of 11.53% occurs for instantaneous *RF* at the end of all cycles. The LSSVM-CSA model shows a better performance in terms of predicting the instantaneous *RF*s at the end of each cycle, as well as the ultimate *RF* at the end of the third cycle. This results in a predicted ultimate RF of 91.57%, compared to the corresponding experimental ultimate *RF* value of 93.58%. The LSSVM-CSA model also outperforms the ANFIS model in terms of computational cost and simulation speed (Table).

The saturation distribution of available phases and the chronological history of phase displacement control the values of three-phase relative permeability and capillary pressure. Therefore, the model performance is greatly influenced by reliability of the capillary pressure and relative permeability models. In the next section, we provide a comparison between the performance of the proposed models to predict the values of the three-phase relative permeability in WAG injection process; we also provide the relative importance analysis for different input parameters.

5.3 Relative importance (RI) of input parameters

To evaluate the impact of each input parameter on the output of a predictive model, the Pearson's correlation (PC) coefficient is used as a measure of the strength of the association between two continuous variables. This coefficient measures the linear correlation between the two variables; it gives information about the magnitude of the association, or correlation, as well as the direction of the relationship between two continuous variables. The PC coefficient is based on the ratio of the covariance of two desired variables to the product of their respective standard deviations [92, 93].

The second coefficient to evaluate the RI of the input parameters is Spearman's correlation (SC) coefficient, which is regarded as the ranked-based version of the PC coefficient. The SC coefficient is a non-parametric measure of the rank correlation, which assesses how well the relationship between the two continuous variables can be defined using a monotonic function [92, 94]. Similar to the PC coefficient, the SC coefficient varies between -1 and +1 and the absolute value of the SC coefficient indicates the strength of the monotonic relationship between the two variables [92]. The closer the absolute value of the SC coefficient to 0, the weaker the monotonic relationship between the two variables. Similar to the PC coefficient, the SC coefficient can be 0 for variables with non-monotonic manner, but unlike the PC coefficient, the SC coefficient can be 1 for both linearly related variables and non-linear variables.

The last rank-order parameter is Kendal's Correlation (KC) coefficient that captures the association between two ordinal (not necessarily interval) variables. The KC coefficient describes the discrepancy between the number of concordant and discordant pairs [92, 94]. The KC coefficient is a measure of the rank correlation; in other words, the similarity of the orderings of

the data when ranked by each of the quantities. The Kendall correlation between two variables is high when observations have a similar rank between the two variables. An example could be the KC coefficient of 1 for an identical rank between the two variables. However, when the observations have a dissimilar rank between the two variables, the KC coefficient has a low magnitude. For instance, it holds the value of -1 when the observations have a fully different rank between the variables. This coefficient can be 1 for a wider range of scenarios, compared to the PC coefficient.

In general, the Relative Importance (RI) can be obtained considering the magnitude of the mentioned coefficients in the [-1, +1] interval. A positive RI value (RI > 0) indicates a positive monotonic association whereas a negative RI value (RI < 0) denotes a negative monotonic association between the variables. In the case of no association between the variables, the RI becomes zero.

Figure 8 shows the impact of each input parameter on the values of the two-phase k_{rw}, k_{ro}, and k_{rg} in gas-water, oil-water, and oil-gas systems, respectively. Since the trend of coefficients for both LSSVM-CSA and ANFIS models are the same, only the data generated by LSSVM-CSA are used in this section. In a two-phase system, the RI values for k_{rwg} and k_{rgw} are the same except for the saturation as the input variable. The trio of all three coefficients i.e. Pearson, Spearman, and Kendal show the same behaviors for all input variables in the three systems. Input parameters with a larger RI values have a greater impact on the output value. In all systems, the saturation imposes the largest impact on the output two-phase relative permeability prediction which is logically sensible. In the gas-water system shown in Figure 8(a), the pressure and temperature have the largest and lowest impacts on the output prediction, respectively. Therefore, changes in pressure results in a comparatively greater change in the relative permeability values. All coefficients are positive for this system, indicating that by increasing each input parameter, the output variable increases. Figure 8(b) depicts the RI value for individual input parameters in the oil-water system to predict oil relative permeability. According to panel (b) of Figure 8, the water saturation has the largest effect on the output variable. Also, all coefficients are negative, meaning that by increasing the water saturation, the oil relative permeability decreases. The water viscosity exhibits the lowest effect on the oil relative permeability, and increasing oil viscosity and rock permeability negatively affect the oil relative permeability (an increase in these parameters leads to a reduction in the oil

relative permeability). In Figure 8(c), the gas saturation is the most influential input parameter in the oil-gas system, while the gas critical saturation is the second important parameter negatively affecting the predicted gas relative permeabilities. In all three cases, the coefficients showed the same trend with a slight difference for each input parameter. However, in different system the sensitivity of coefficients might be different for different input variables. For instance, in the panel "c", for all input parameters, the Spearman coefficient shows more *RI* variations compared to the Kendal and Pearson coefficients. However, the Pearson coefficient in the same panel exhibits less sensitivity of *RI* to the variables, and results in almost the same values for critical gas saturation, permeability, and porosity of the system.

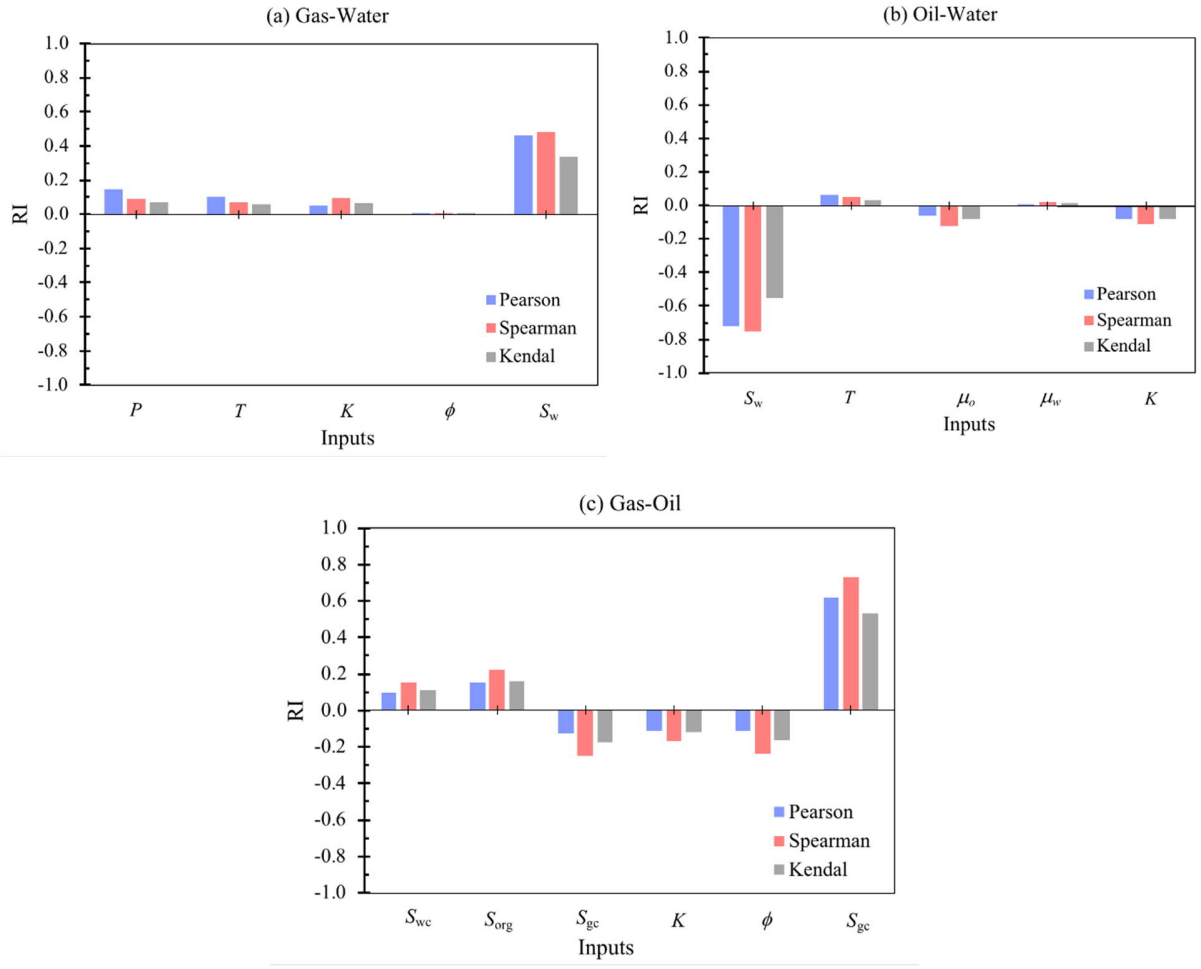

Figure 8: Calculated relative importance of each input parameter in the (a) gas-water, (b) oil-water, and (c) gas-oil flow system to predict water relative permeability using LSSVM-CSA model.

5.4 Three-phase relative permeability comparison

The accurate estimation of the three-phase relative permeability values, which is one of the main objectives of this study, is crucial for reliably evaluating the performance of the WAG injection process. In this section, the oil, water, and gas relative permeabilities, obtained using all the proposed smart models as well as the numerical simulation model, for all the gas and water injection cycles associated with the WAG injection case study are presented. For this purpose, first, the two-phase relative permeability values are calculated using EM's as well as ANFIS and LSSVM-CSA algorithms over the same range of saturations experienced in the experimental work. Then, the three-phase relative permeability values are determined using the model developed by Shahverdi et al. [16] (Eqs. (1)– (3)) by incorporating the two-phase relative permeability data. In all the plots, the experimental three-phase relative permeability values are also presented for comparison purposes.

Three-phase relative permeability data in GI cycles. In **Figure 9**, the three-phase gas relative permeability (K_{rg}^{3ph}) values obtained using the proposed models for the first, second, and third gas injection cycles of the WAG injection case study are plotted, along with the experimental data. It is clear that as the injection process proceeds, the K_{rg}^{3ph} value significantly decreases at corresponding gas saturation values. This can be attributed to the dependency of the K_{rg}^{3ph} on the saturation history in a water-wet medium. Even though the same drainage displacement process takes place during GI1, GI2 and GI3 stages, the successively decreasing K_{rg}^{3ph} values at similar gas saturation levels reveals the importance of periodic displacement transition from imbibition to drainage on magnitude of the non-wetting phase relative permeability. Of particular importance, among all other reasons, could be the blockage of the free gas phase by invading water phase during the prior imbibition stage(s). This apparently irreversible gas trapping restricts the flow of free gas in the next gas injection cycle, which results in K_{rg}^{3ph} reduction.

As for the reliability of the K_{rg}^{3ph} predictions, the ANFIS model is clearly the least reliable predictive tool, whereas the correlation-based EM results in the best fit to the experimental data. The discrepancy between the predicted and measured K_{rg}^{3ph} data is more pronounced at lower gas

saturation values. As the initial gas saturation in the porous medium increases from GI1 to GI3 stage, the accuracy of the models predictions with respect to the measured values increases.

A comparison between the predicted versus measured three-phase water relative permeability (K_{rw}^{3ph}) values during the gas injection cycles is presented in Figure 9. The changes in the K_{rw}^{3ph} values between the GI1 and GI2 stages over the same range of water saturations are minimal, showing that the saturation history does not play an important role. However, the K_{rw}^{3ph} values in GI3 decrease by about 30% compared to the corresponding values in the previous two gas injection stages. At smaller water saturation values, all the predictive models overestimate the K_{rw}^{3ph} values when compared to the experimental data. However, at greater water saturation values, the deviation of the predictions from the measured values becomes negligible. The best K_{rw}^{3ph} predictions are obtained using the correlation-based EM over the entire range of water saturations while the estimations with the lowest accuracy belong to the ANFIS model, especially at lower ranges of water saturation.

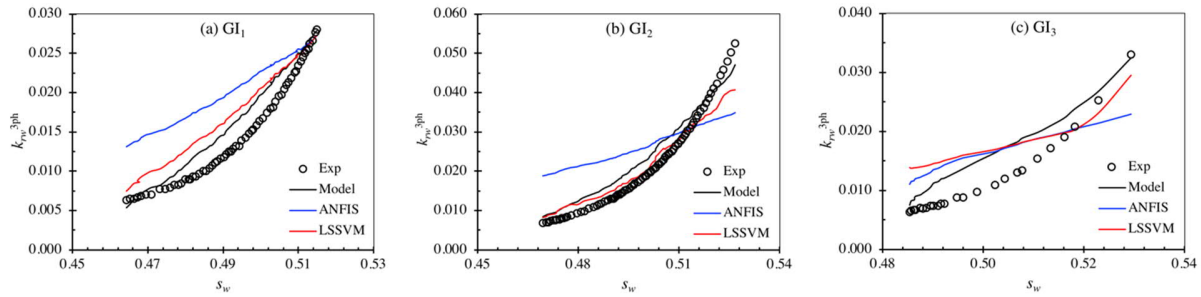

Figure 9: Comparison of the K_{rw}^{3ph} values in the (a) first, (b) second, and (c) third GI cycles using correlation-based EM as well as ANFIS, and LSSVM-CSA algorithms.

In the GI cycles, the three-phase oil relative permeability (K_{ro}^{3ph}) values predicted by the proposed models are also compared with the experimental data (see Figure 10). The oil phase is mobilized at less oil saturation levels through consecutive GI cycles, which is due to the decrease in oil saturation in porous medium while conducting further WAG injection cycles. The effect of saturation history on K_{ro}^{3ph} values is also evident in Figure 10, and the transition between the imbibition and drainage processes in each cycle remarkably improves the K_{ro}^{3ph} values and

successively decreases the residual oil saturation through consecutive injection cycles. Similar to the case of K_{rw}^{3ph} and K_{rg}^{3ph}, the K_{ro}^{3ph} experimental data are best fitted with the correlation-based EM. However, the ANFIS and LSSVM-CSA models have similar predictive performance while obtaining K_{ro}^{3ph} data. All the proposed ANN models underestimate the K_{ro}^{3ph} values at lower oil saturations, especially when approaching the residual oil saturation conditions. This might be due to the wettability alteration of the rock towards the less water-wet state during the gas injection cycles at the experimental temperature and pressure. The used models do not account for the changes in the rock and fluid properties, which results in smaller K_{ro}^{3ph} values during the gas injection stages.

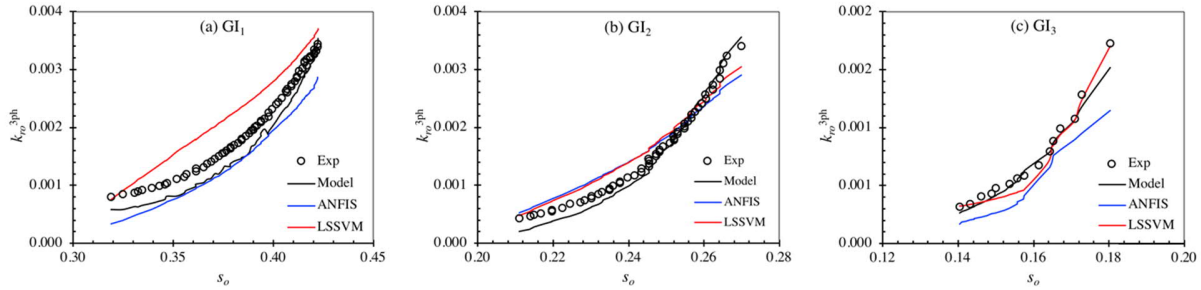

Figure 10: Comparison of the K_{ro}^{3ph} values in the (a) first, (b) second, and (c) third GI cycles using correlation-based model as well as ANFIS and LSSVM-CSA algorithms.

Three-phase relative permeability data during WI stages. The relative permeability predictions during the WI stages are depicted in Figure 11-13. During the WI1 stage, only water and oil are present in the porous medium; therefore, the two-phase oil-water relative permeability data are presented in Figures 11(a), 12(a) and 13(a).

Unfortunately, the experimental data are not available for the WI stages. Therefore, for the comparison purposes, we select the correlation-based EM predictions as the baseline relative permeability data owing to its excellent performance (it accurately predicts the experimental results obtained in the GI stages). We compare the relative permeability values predicted by the ANFIS and LSSVM-CSA models during WI stages with the results obtained from the EM model as our baseline. Both the ANFIS and LSSVM-CSA models are in good agreement with the baseline relative permeability curve during the first WI stages for oil, water, and gas (Figures 11(a), 12(a) and 13(a)). However, in the second and third WI stages, the ANFIS and LSSVM-CSA models lead to less accurate three-phase relative permeability values compared to the baseline correlation-

based EM. During the WI stages, the same common trends in relative permeability data are observed as those in the GI stages. For instance, the importance of cyclic displacement process transition from imbibition to drainage is evident in mobilizing the lower oil saturations as the WAG injection process proceeds (see panels (b) and (c) of Figure 11). This also depicts itself in successively decreasing residual oil saturation values through the cyclic injection stages. Figure 12 demonstrates that the end-point water relative permeability value during WI2 and WI3 stages does not significantly vary. The LSSVM-CSA model performs well in following the trend and values of the baseline data as depicted in all two- and three-phase relative permeability plots. The effect of saturation history on K_{rg}^{3ph} during the WI stages (Figures 13(a) and 13(b)) is significant, resulting in reduced gas relative permeability at similar saturation levels. The residual gas saturation subsequently decreases over the WI stages. The results given in Figure 11 and Figure 13 also reveal that the oil and gas relative permeabilities during the WI2 and WI3 cycles considerably decrease as the water breakthrough occurs. This is more significant in the case of gas relative permeability (Figure 13) during the WI2 and WI3 cycles, when the gas saturation change is negligible after the water breakthrough.

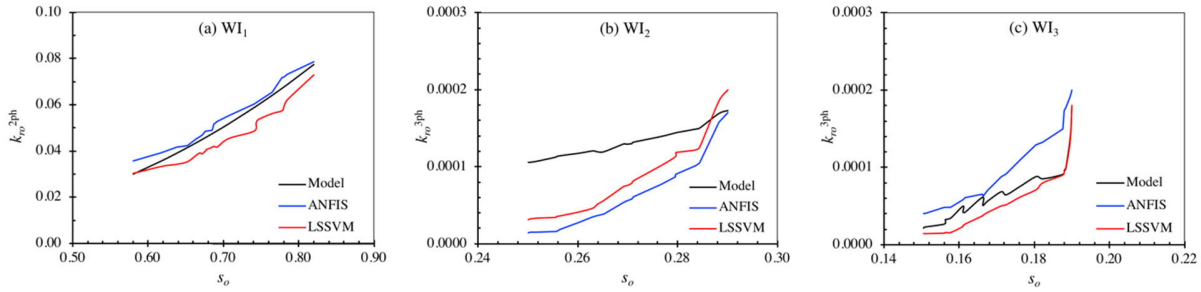

Figure 11: Comparison of the K_{ro}^{3ph} values in the (a) first, (b) second, and (c) third WI cycles using correlation-based EM as well as ANFIS and LSSVM-CSA algorithms (Note: due to zero gas saturation during WI1 stage, the (a) plot expresses the two-phase oil relative permeability data).

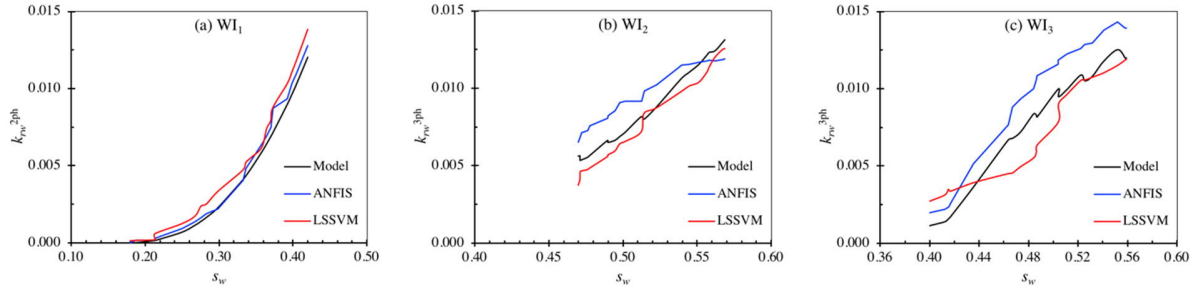

Figure 12: Comparison of the K_{rw}^{3ph} values in the (a) first, (b) second, and (c) third WI stages using correlation-based EM as well as ANFIS and LSSVM-CSA algorithms (Note: due to zero gas saturation during WI1 stage, the (a) plot expresses the two-phase water relative permeability data).

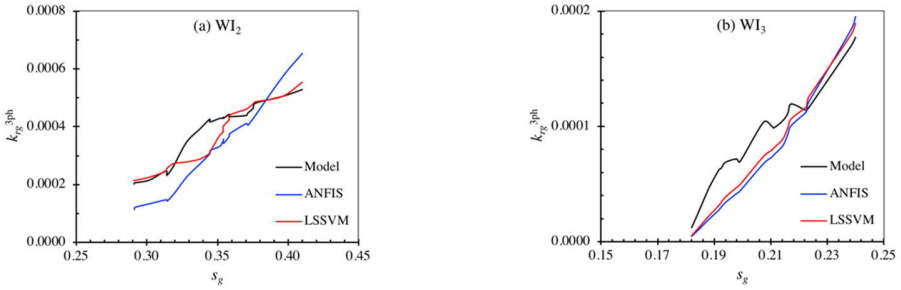

Figure 13: Comparison of the K_{rg}^{3ph} data in (a) first, (b) second, and (c) third WI stages using correlation-based EM as well as ANFIS and LSSVM-CSA algorithms.

6 Summary and Conclusions

In the current study, we use various hybrid models to predict the three-phase relative permeability data for a high-pressure WAG injection experiment. The LSSVM-CSA and ANFIS models are employed to predict the two-phase relative permeability curves, and then a three-phase relative permeability correlation is used with input values from the two-phase data. In another effort, the we used the two-phase relative permeability empirical models by Mualem [84] and Hirasaki [85] to obtain the two-phase data, which are then implemented in the three-phase relative permeability correlation model. To assess the reliability of the predictions, the instantaneous and ultimate RF values, along with the relative permeability data are selected as the objective functions to be compared against the experimental data. The experimental data are taken from the literature, for a water-wet Berea sandstone core at temperature and pressure equal to 38 ^{o}C and 12.7 MPa, respectively. The following conclusions are drawn based on this study:

- The statistical quality measures reveal that the LSSVM-CSA and ANFIS models can be successfully trained for relative permeability predictions with relatively small errors.
- The LSSVM-CSA model exhibits a better predictive performance by generating less errors (RMSE, Mean Error, and Error_std) associated with the training, testing, and validating stages for the two-phase flow systems.

- The correlation-based EM as well as the LSSVM-CSA and ANFIS algorithms used in this study predict the ultimate RF values of 92%, 91.57%, and 82.88%, respectively, in comparison with the experimental measured value of 93.58% at the end of the WAG injection process.
- According to the PC, SC, and KC coefficients in the gas-water system, the pressure and temperature have the largest and lowest impacts on the output predictions, respectively. All coefficients are positive for this system, indicating that by increasing each input parameter, the output variable increases.
- The RI analysis of oil-water system shows that the water viscosity has the lowest impact on two-phase relative permeability values and water saturation, oil viscosity, and rock permeability negatively influence oil relative permeability meaning that by increasing these parameters, the oil relative permeability decreases and vice versa.
- The gas saturation is the most influential input parameter in the oil-gas system, while the gas critical saturation is the second influential parameter; it negatively affects on the predicted gas relative permeabilities (similar to the rock permeability and porosity).
- The best fit to the experimental three-phase relative permeability data is attained by correlation-based EM, while the ANFIS model leads to the less-accurate predictions.
- The three-phase water relative permeability values in three GI and WI cycles show less hysteresis compared to the gas relative permeabilities.
- The amount of residual oil saturations at the end of each WI or GI stage has a decreasing trend due to the cyclic nature of the saturation history transition between the imbibition and drainage processes during the WAG injection process.

Acknowledgements

The authors would like to acknowledge the financial support provided by Memorial University (NL, Canada), Natural Sciences and Engineering Research Council of Canada (NSERC), InnovateNL, and Equinor Canada.

Nomenclatures

Acronyms

ANN	Artificial neural network
ANFIS	Adaptive neuro-fuzzy inference system
Cost	Cost function
CSA	Coupled simulated annealing
EOR	Enhanced oil recovery
EM	Empirical model
FIS	Fuzzy inference system
FPM	First principal model
GI	Gas injection
IFT	Interfacial tension
IOR	Improved oil recovery
IWAG	Immiscible WAG
IMPES	Implicit-pressure-explicit-saturation
LSSVM	Least square support vector machine
ME	Mean error
MF	Membership function
MMP	Minimum miscibility pressure
PVI	Pore volume injection
PC	Pearson’s coefficient
RBF	Radial basis kernel function
RF	Recovery factor
RI	Relative importance
RMSE	Root mean square error

SC	Spearman's coefficient
Std	Standard deviation
SVM	Support vector machine
WI	Water injection
WAG	Water-alternating-gas injection

Variables and Parameters

a	Capillary exponent
b	Bias term
c	Capillary entry pressure
K	Absolute permeability
k_{ri}	Relative permeability of phase i
k_{ri}^{o}	Endpoint elative permeability of phase i
p	Pressure
Q	Membership function
s_i	Saturation of phase i
s_{ic}	Critical saturation of phase i
t	Time
T	Temperature
w	Weight factor
x	Length

Greek Letters

μ	Viscosity
μ_{Ai}	Generalized bell function
ρ	Density
σ	Variance of the Gaussian function
ϕ	Porosity
θ	Contact angle
ζ	Regression error
ψ	Non-linear function

Subscripts and Superscripts

C	Capillary pressure
D	Drainage
g	Gas phase
I	Imbibition
o	Oil phase
og	Oil-gas system
org	Residual oil after GI
ow	Oil-water system
w	Water phase
wg	Water-gas system
r	Residual phase

References

[1] O.A. Talabi, J.E. Moreno, R.K. Malhotra, Y. Liu, Practical Upscaling of WAG Hysteresis Parameters from Core to Full-Field Scale Part II, in: SPE/IATMI Asia Pacific Oil & Gas Conference and Exhibition, Society of Petroleum Engineers, 2019.
[2] M. Sherafati, K. Jessen, Dynamic relative permeability and Simulation of WAG injection processes, Transport in Porous Media, 117 (2017) 125-147.
[3] S. Aghabozorgi, M. Sohrabi, J. Facanha, Estimation of Three-phase Oil Relative Permeability in WAG Experiments, in: Offshore Technology Conference Brasil, Offshore Technology Conference, 2019.
[4] L. Moghadasi, E. Ranaee, D. Renna, M. Bartosek, G. Maddinelli, F. Masserano, A. Cominelli, F. Inzoli, A. Guadagnini, Combining Two-and Three-Phase Coreflooding Experiments for Reservoir Simulation Under WAG Practices, in: International Petroleum Technology Conference, International Petroleum Technology Conference, 2020.
[5] F.M. Carlson, Simulation of relative permeability hysteresis to the nonwetting phase, in: SPE annual technical conference and exhibition, Society of Petroleum Engineers, 1981.
[6] C.S. Land, Calculation of imbibition relative permeability for two-and three-phase flow from rock properties, Society of Petroleum Engineers Journal, 8 (1968) 149-156.
[7] K. Aziz, A. Settari, Petroleum reservoir simulation: Applied science publ, Ltd., London, (1979).
[8] J.D. Rogers, R.B. Grigg, A literature analysis of the WAG injectivity abnormalities in the CO2 process, SPE Reservoir Evaluation & Engineering, 4 (2001) 375-386.
[9] A. Skauge, J.A. Larsen, Three-phase relative permeabilities and trapped gas measurements related to WAG processes, in: SCA 9421, proceedings of the International Symposium of the Society of Core Analysts, Stavanger, Norway, 1994.
[10] J. Larsen, A. Skauge, Methodology for numerical simulation with cycle-dependent relative permeabilities, SPE Journal, 3 (1998) 163-173.

[11] P. Egermann, O. Vizika, L. Dallet, C. Requin, F. Sonier, Hysteresis in three-phase flow: experiments, modeling and reservoir simulations, in: SPE European petroleum conference, Society of Petroleum Engineers, 2000.
[12] A.T. Corey, C. Rathjens, J. Henderson, M. Wyllie, Three-phase relative permeability, Journal of Petroleum Technology, 8 (1956) 63-65.
[13] C.S. Land, Comparison of calculated with experimental imbibition relative permeability, Society of Petroleum Engineers Journal, 11 (1971) 419-425.
[14] H. Stone, Estimation of three-phase relative permeability and residual oil data, Journal of Canadian Petroleum Technology, 12 (1973).
[15] M. Delshad, M. Delshad, G. Pope, L. Lake, Two-and three-phase relative permeabilities of micellar fluids, SPE Formation Evaluation, 2 (1987) 327-337.
[16] H. Shahverdi, M. Sohrabi, Three-phase relative permeability and hystresis model for simulation of water alternating gas (WAG) injection, in: SPE Improved Oil Recovery Symposium, Society of Petroleum Engineers, 2012.
[17] H.G. Botset, Flow of gas-liquid mixtures through consolidated sand, Transactions of the AIME, 136 (1940) 91-105.
[18] I. Fatt, The network model of porous media, Transactions of the AIME, 207 (1956) 144-181.
[19] G.L. Stegemeier, The relationship of relative permeability to contact angles, in, University of Texas at Austin, 1954.
[20] M. Muskat, R. Wyckoff, H. Botset, M. Meres, Flow of gas-liquid mixtures through sands, Transactions of the AIME, 123 (1937) 69-96.
[21] M. Leverett, W. Lewis, Steady flow of gas-oil-water mixtures through unconsolidated sands, Transactions of the AIME, 142 (1941) 107-116.
[22] S. Esmaeili, H. Sarma, T. Harding, B. Maini, A data-driven model for predicting the effect of temperature on oil-water relative permeability, Fuel, 236 (2019) 264-277.
[23] V. Vapnik, The nature of statistical learning theory, Springer science & business media, 2013.

[24] T.H. Hann, E. Steurer, Much ado about nothing? Exchange rate forecasting: Neural networks vs. linear models using monthly and weekly data, Neurocomputing, 10 (1996) 323-339.
[25] S. Rafiee-Taghanaki, M. Arabloo, A. Chamkalani, M. Amani, M.H. Zargari, M.R. Adelzadeh, Implementation of SVM framework to estimate PVT properties of reservoir oil, Fluid Phase Equilibria, 346 (2013) 25-32.
[26] A. Shokrollahi, M. Arabloo, F. Gharagheizi, A.H. Mohammadi, Intelligent model for prediction of CO2–reservoir oil minimum miscibility pressure, Fuel, 112 (2013) 375-384.
[27] E.D. Übeyli, Least squares support vector machine employing model-based methods coefficients for analysis of EEG signals, Expert Systems with Applications, 37 (2010) 233-239.
[28] J. Suykens, Support Vector Machines and Kernel Based Learning, Tutorial: IJCNN, Montreal,[Online], Available from:< http://www. esat. kuleuven. ac. be/sista/lssvmlab/ijcnn2005_4. pdf, (2003).
[29] J.A. Suykens, J. Vandewalle, Least squares support vector machine classifiers, Neural processing letters, 9 (1999) 293-300.
[30] S. Nowroozi, M. Ranjbar, H. Hashemipour, M. Schaffie, Development of a neural fuzzy system for advanced prediction of dew point pressure in gas condensate reservoirs, Fuel Processing Technology, 90 (2009) 452-457.
[31] A. Fayazi, M. Arabloo, A. Shokrollahi, M.H. Zargari, M.H. Ghazanfari, State-of-the-art least square support vector machine application for accurate determination of natural gas viscosity, Industrial & Engineering Chemistry Research, 53 (2014) 945-958.
[32] S. Sinehbaghizadeh, A. Roosta, N. Rezaei, M.M. Ghiasi, J. Javanmardi, S. Zendehboudi, Evaluation of phase equilibrium conditions of clathrate hydrates using connectionist modeling strategies, Fuel, 255 (2019) 115649.
[33] H. Yarveicy, A.K. Moghaddam, M.M. Ghiasi, Practical use of statistical learning theory for modeling freezing point depression of electrolyte solutions: LSSVM model, Journal of Natural Gas Science and Engineering, 20 (2014) 414-421.

[34] A. Shokrollahi, M. Arabloo, F. Gharagheizi, A.H. Mohammadi, Intelligent model for prediction of CO2 – Reservoir oil minimum miscibility pressure, Fuel, 112 (2013) 375-384.
[35] M.N.M. Salleh, N. Talpur, K. Hussain, Adaptive Neuro-Fuzzy Inference System: Overview, Strengths, Limitations, and Solutions, in: International Conference on Data Mining and Big Data, Springer, 2017, pp. 527-535.
[36] S. Kar, S. Das, P.K. Ghosh, Applications of neuro fuzzy systems: A brief review and future outline, Applied Soft Computing, 15 (2014) 243-259.
[37] K. Hussain, M. Salleh, M. Najib, Analysis of techniques for anfis rule-base minimization and accuracy maximization, (2015).
[38] J.-S. Jang, ANFIS: adaptive-network-based fuzzy inference system, IEEE transactions on systems, man, and cybernetics, 23 (1993) 665-685.
[39] A. Rostami, A. Baghban, A.H. Mohammadi, A. Hemmati-Sarapardeh, S. Habibzadeh, Rigorous prognostication of permeability of heterogeneous carbonate oil reservoirs: Smart modeling and correlation development, Fuel, 236 (2019) 110-123.
[40] H. Zargari, S. Poordad, R. Kharrat, Porosity and permeability prediction based on computational intelligences as artificial neural networks (ANNs) and adaptive neuro-fuzzy inference systems (ANFIS) in southern carbonate reservoir of Iran, Petroleum science and technology, 31 (2013) 1066-1077.
[41] A. Karkevandi-Talkhooncheh, M. Sharifi, M. Ahmadi, Application of hybrid adaptive neuro-fuzzy inference system in well placement optimization, Journal of Petroleum Science and Engineering, 166 (2018) 924-947.
[42] M. Wei, B. Bai, A.H. Sung, Q. Liu, J. Wang, M.E. Cather, Predicting injection profiles using ANFIS, Information Sciences, 177 (2007) 4445-4461.
[43] A. Barati-Harooni, A. Najafi-Marghmaleki, Implementing a PSO-ANFIS model for prediction of viscosity of mixed oils, Petroleum Science and Technology, 35 (2017) 155-162.
[44] A. Karkevandi-Talkhooncheh, S. Hajirezaie, A. Hemmati-Sarapardeh, M.M. Husein, K. Karan, M. Sharifi, Application of adaptive

neuro fuzzy interface system optimized with evolutionary algorithms for modeling CO2-crude oil minimum miscibility pressure, Fuel, 205 (2017) 34-45.
[45] I. Rahimzadeh Kivi, M. Ameri Shahrabi, M. Akbari, The development of a robust ANFIS model for predicting minimum miscibility pressure, Petroleum science and technology, 31 (2013) 2039-2046.
[46] E. Keybondorian, A. Taherpour, A. Bemani, T. Hamule, Application of novel ANFIS-PSO approach to predict asphaltene precipitation, Petroleum Science and Technology, 36 (2018) 154-159.
[47] H.A. Zamani, S. Rafiee-Taghanaki, M. Karimi, M. Arabloo, A. Dadashi, Implementing ANFIS for prediction of reservoir oil solution gas-oil ratio, Journal of Natural Gas Science and Engineering, 25 (2015) 325-334.
[48] A.A. Mahmoud, S. Elkatatny, W. Chen, A. Abdulraheem, Estimation of oil recovery factor for water drive sandy reservoirs through applications of artificial intelligence, Energies, 12 (2019) 3671.
[49] M. Babanezhad, A.T. Nakhjiri, S. Shirazian, Changes in the number of membership functions for predicting the gas volume fraction in two-phase flow using grid partition clustering of the ANFIS method, ACS omega, 5 (2020) 16284-16291.
[50] M. Babanezhad, S. Zabihi, I. Behroyan, A.T. Nakhjiri, A. Marjani, S. Shirazian, Prediction of gas velocity in two-phase flow using developed fuzzy logic system with differential evolution algorithm, Scientific reports, 11 (2021) 1-14.
[51] M. Babanezhad, A.T. Nakhjiri, A. Marjani, M. Rezakazemi, S. Shirazian, Evaluation of product of two sigmoidal membership functions (psigmf) as an ANFIS membership function for prediction of nanofluid temperature, Scientific Reports, 10 (2020) 22337.
[52] M. Babanezhad, I. Behroyan, A.T. Nakhjiri, A. Marjani, S. Shirazian, Performance and application analysis of ANFIS artificial intelligence for pressure prediction of nanofluid convective flow in a heated pipe, Scientific Reports, 11 (2021) 902.
[53] M. Babanezhad, I. Behroyan, A.T. Nakhjiri, M. Rezakazemi, A. Marjani, S. Shirazian, Thermal prediction of turbulent forced convection

of nanofluid using computational fluid dynamics coupled genetic algorithm with fuzzy interface system, Scientific Reports, 11 (2021) 1308.
[54] M. Babanezhad, I. Behroyan, A. Marjani, S. Shirazian, Velocity prediction of nanofluid in a heated porous pipe: DEFIS learning of CFD results, Scientific Reports, 11 (2021) 1-11.
[55] M. Babanezhad, A. Taghvaie Nakhjiri, M. Rezakazemi, A. Marjani, S. Shirazian, Functional input and membership characteristics in the accuracy of machine learning approach for estimation of multiphase flow, Scientific Reports, 10 (2020) 17793.
[56] A. Kamari, A. Bahadori, A.H. Mohammadi, S. Zendehboudi, Evaluating the unloading gradient pressure in continuous gas-lift systems during petroleum production operations, Petroleum science and technology, 32 (2014) 2961-2968.
[57] R. Roghanian, S. Asadolahpour, M. Rasaei, The prediction of water-oil relative permeability key points using an adaptive neuro-fuzzy inference system, Petroleum science and technology, 32 (2014) 2004-2019.
[58] S.R. Amendolia, G. Cossu, M.L. Ganadu, B. Golosio, G.L. Masala, G.M. Mura, A comparative study of K-Nearest Neighbour, Support Vector Machine and Multi-Layer Perceptron for Thalassemia screening, Chemometrics and Intelligent Laboratory Systems, 69 (2003) 13-20.
[59] M.M. Ghiasi, Z. Esmaeili-Jaghdan, M.A. Halali, M. Lee, A. Abbas, A. Bahadori, Development of soft computing methods to predict moisture content of natural gases, Journal of the Taiwan Institute of Chemical Engineers, 55 (2015) 36-41.
[60] M.M. Ghiasi, A.H. Mohammadi, Determination of methane-hydrate phase equilibrium in the presence of electrolytes or organic inhibitors by using a semi-theoretical framework, Energy Technology, 1 (2013) 519-529.
[61] M.M. Ghiasi, M. Arabloo, A. Bahadori, S. Zendehboudi, Prediction of methanol loss in liquid hydrocarbon phase during natural gas hydrate inhibition using rigorous models, Journal of Loss Prevention in the Process Industries, 33 (2015) 1-9.
[62] C. Cortes, V. Vapnik, Support-vector networks, Machine Learning, 20 (1995) 273-297.

[63] J. De Brabanter, B. De Moor, J.A. Suykens, T. Van Gestel, J.P. Vandewalle, Least squares support vector machines, World scientific, 2002.
[64] M. Seyyedattar, M.M. Ghiasi, S. Zendehboudi, S. Butt, Determination of bubble point pressure and oil formation volume factor: Extra trees compared with LSSVM-CSA hybrid and ANFIS models, Fuel, (2020) 116834.
[65] M.M. Ghiasi, A. Bahadori, A NEW CORRELATION FOR ACCURATE ESTIMATION OF NATURAL GASES WATER CONTENT, Petroleum & Coal, 56 (2014).
[66] M.M. Ghiasi, A. Hajinezhad, H. Yousefi, A.H. Mohammadi, CO2 loading capacity of DEA aqueous solutions: Modeling and assessment of experimental data, International Journal of Greenhouse Gas Control, 56 (2017) 289-301.
[67] H. Saghafi, M.M. Ghiasi, A.H. Mohammadi, CO2 capture with aqueous solution of sodium glycinate: Modeling using an ensemble method, International Journal of Greenhouse Gas Control, 62 (2017) 23-30.
[68] M.M. Ghiasi, A.H. Mohammadi, Development of reliable models for determination of required monoethanolamine (MEA) circulation rate in amine plants, Separation Science and Technology, 50 (2015) 2248-2256.
[69] L.-C. Ying, M.-C. Pan, Using adaptive network based fuzzy inference system to forecast regional electricity loads, Energy Conversion and Management, 49 (2008) 205-211.
[70] F. Ameli, A. Hemmati-Sarapardeh, A. Tatar, A. Zanganeh, S. Ayatollahi, Modeling interfacial tension of normal alkane-supercritical CO2 systems: Application to gas injection processes, Fuel, 253 (2019) 1436-1445.
[71] H. Yang, Z. Xu, M. Fan, R. Gupta, R.B. Slimane, A.E. Bland, I. Wright, Progress in carbon dioxide separation and capture: A review, Journal of environmental sciences, 20 (2008) 14-27.
[72] A. Kamari, A. Safiri, A.H. Mohammadi, Compositional model for estimating asphaltene precipitation conditions in live reservoir oil systems, Journal of Dispersion Science and Technology, 36 (2015) 301-309.

[73] A. Dashti, M. Raji, A. Razmi, N. Rezaei, S. Zendehboudi, M. Asghari, Efficient hybrid modeling of CO2 absorption in aqueous solution of piperazine: Applications to energy and environment, Chemical Engineering Research and Design, 144 (2019) 405-417.
[74] L. Surguchev, R. Korbol, S. Haugen, O. Krakstad, Screening of WAG injection strategies for heterogeneous reservoirs, in: European petroleum conference, Society of Petroleum Engineers, 1992.
[75] S.A.R. Tabatabaei Nezhad, M. Rahimzadeh Mojarad, P. Oskouei, S. Javad, J.S. Moghadas, D.R. Farahmand, Experimental Study on Applicability of Water Alternating CO2 Injection in the Secondary and Tertiary Recovery, in: International Oil Conference and Exhibition in Mexico, Society of Petroleum Engineers, 2006.
[76] S. Afzali, A. Ghamartale, N. Rezaei, S. Zendehboudi, Mathematical modeling and simulation of water-alternating-gas (WAG) process by incorporating capillary pressure and hysteresis effects, Fuel, (2019) 116362.
[77] E. Braun, R. Holland, Relative permeability hysteresis: Laboratory measurements and a conceptual model, SPE Reservoir Engineering, 10 (1995) 222-228.
[78] J. Osoba, J. Richardson, J. Kerver, J. Hafford, P. Blair, Laboratory measurements of relative permeability, Journal of Petroleum Technology, 3 (1951) 47-56.
[79] S.A. Bradford, F.J. Leij, Predicting two-and three-fluid capillary pressure-saturation relationships of porous media with fractional wettability, Water Resources Research, 32 (1996) 251-259.
[80] P. Egermann, K. Mejdoub, J.-M. Lombard, O. Vizika, Z. Kalam, Drainage three-phase flow relative permeability on oil-wet carbonate reservoir rock types: Experiments, interpretation and comparison with standard correlations, Petrophysics, 55 (2014) 287-293.
[81] M. Oak, Three-phase relative permeability of intermediate-wet Berea sandstone, in: SPE Annual Technical Conference and Exhibition, Society of Petroleum Engineers, 1991.
[82] M. Van Dijke, K. Sorbie, S. McDougall, Saturation-dependencies of three-phase relative permeabilities in mixed-wet and fractionally wet systems, Advances in Water Resources, 24 (2001) 365-384.

[83] H. Shahverdi, M. Sohrabi, An improved three-phase relative permeability and hysteresis model for the simulation of a water-alternating-gas injection, Spe Journal, 18 (2013) 841-850.
[84] Y. Mualem, A new model for predicting the hydraulic conductivity of unsaturated porous media, Water resources research, 12 (1976) 513-522.
[85] G.J. Hirasaki, Sensitivity coefficients for history matching oil displacement processes, Society of Petroleum Engineers Journal, 15 (1975) 39-49.
[86] T.H. Ahmed, Comparative study of eight equations of state for predicting hydrocarbon volumetric phase behavior, SPE Reservoir Engineering, 3 (1988) 337-348.
[87] M.M. Ghiasi, S. Zendehboudi, Decision tree-based methodology to select a proper approach for wart treatment, Computers in biology and medicine, 108 (2019) 400-409.
[88] F. Gharagheizi, A. Eslamimanesh, A.H. Mohammadi, D. Richon, Artificial neural network modeling of solubilities of 21 commonly used industrial solid compounds in supercritical carbon dioxide, Industrial & engineering chemistry research, 50 (2011) 221-226.
[89] H. Hamedi, M. Ehteshami, S.A. Mirbagheri, S. Zendehboudi, New deterministic tools to systematically investigate fouling occurrence in membrane bioreactors, Chemical Engineering Research and Design, 144 (2019) 334-353.
[90] S. Zendehboudi, N. Rezaei, A. Lohi, Applications of hybrid models in chemical, petroleum, and energy systems: A systematic review, Applied Energy, 228 (2018) 2539-2566.
[91] S.M. Fatemi, Multiphase flow and hysteresis phenomena in oil recovery by water alternating gas (WAG) injection, in, Heriot-Watt University, 2015.
[92] N.S. Chok, Pearson's versus Spearman's and Kendall's correlation coefficients for continuous data, in, University of Pittsburgh, 2010.
[93] A. Tatar, G.M. Moghtadaei, A. Manafi, I. Cachadiña, Á. Mulero, Determination of pure alcohols surface tension using Artificial Intelligence methods, Chemometrics and Intelligent Laboratory Systems, 201 (2020) 104008.

[94] A. Tatar, G.M. Moghtadaei, A. Manafi, I. Cachadiña, Á. Mulero, Determination of pure alcohols surface tension using Artificial Intelligence methods, Chemometrics and Intelligent Laboratory Systems, (2020) 104008.